arXiv:astro-ph/0301454v2 25 Jun 2003

February 2, 2008

Quantitative Spectroscopy of O Stars at Low Metallicity. O Dwarfs in NGC 346.[1]

J.-C. Bouret[2], T. Lanz[3,4], D. J. Hillier[5], S. R. Heap[3], I. Hubeny[3,6], D. J. Lennon[7], L. J. Smith[8], and C. J. Evans[7,8]

Jean-Claude.Bouret@astrsp-mrs.fr

lanz@stars.gsfc.nasa.gov

ABSTRACT

We present the results of a detailed analysis of the properties of dwarf O-type stars in a metal-poor environment. High-resolution, high-quality, ultraviolet and optical spectra of six O-type stars in the H II region NGC 346 have been obtained from a spectroscopic survey of O stars in the SMC. Stellar parameters and chemical abundances have been determined using NLTE line-blanketed photospheric models calculated with TLUSTY. Additionally, we have modeled the spectra with the NLTE line-blanketed wind code, CMFGEN, to derive wind parameters. Stellar parameters and chemical abundances, and in particular iron abundances, obtained with the two NLTE codes compare quite favorably. This

[1]Based on observations with the NASA/ESA Hubble Space Telescope, obtained at the Space Telescope Science Institute, which is operated by the Association of Universities for Research in Astronomy, Inc., under NASA contract NAS5-2655. Also based on observations obtained at the European Southern Observatory (La Silla) and at the Anglo-Australian Observatory (Siding Spring).

[2]Laboratoire d'Astrophysique de Marseille, Traverse du Siphon - BP 8, 13376 Marseille Cedex 12, France

[3]NASA Goddard Space Flight Center, Code 681, Greenbelt, MD 20771

[4]Department of Astronomy, University of Maryland, College Park, MD 20742

[5]Department of Physics and Astronomy, University of Pittsburgh, Pittsburgh, PA 15260

[6]National Optical Astronomy Observatories, Tucson, AZ 85726

[7]Isaac Newton Group, Apartado 321, 38700 Santa Cruz de La Palma, Canary Islands, Spain

[8]Department of Physics and Astronomy, University College London, Gower Street, London WC1E 6BT, UK

consistency demonstrates that basic photospheric parameters of main-sequence O stars can be reliably determined using NLTE static model atmospheres. With the two NLTE codes, we need to introduce a microturbulent velocity in order to match the observed spectra. Our results hint at a decrease of the required microturbulent velocity from a value close to the sonic velocity in early O stars to a low value in late O stars. Similarly to several recent studies of Galactic, LMC and SMC stars, we derive effective temperatures lower than predicted from the widely-used relation between spectral type and $T_{\rm eff}$, resulting in lower stellar luminosities and lower ionizing fluxes. From evolutionary tracks in the HR diagram, we find an age of $3\,10^6$ years for NGC 346. A majority of the stars in our sample reveal CNO-cycle processed material at their surface during the main-sequence stage, indicating thus fast stellar rotation and/or very efficient mixing processes. We obtain an overall metallicity, $Z = 0.2Z_{\odot}$, in good agreement with other recent analyses of SMC stars. We study the dependence of the mass loss rate with the stellar metallicity and find a satisfactory agreement with recent theoretical predictions for three most luminous stars of the sample. The wind-momentum luminosity relation for our sample stars derived for these stars agree with previous studies. However, the three other stars of our sample reveal very weak signatures of mass loss. We obtain mass loss rates that are significantly lower than $10^{-8}\,{\rm M}_{\odot}\,{\rm yr}^{-1}$, which is below the predictions of radiative line-driven wind theory by an order of magnitude or more. Furthermore, evidence of clumping in the wind of main-sequence of O stars is provided by O V λ1371. Like previous studies of O star winds, we are unable to reproduce this line with homogeneous wind models, but we have achieved very good fits with clumped models. Clumped wind models systematically yield lower mass loss rates than theoretical predictions.

Subject headings: Stars: abundances, atmospheres, early-type, fundamental parameters, mass loss – Small Magellanic Cloud

1. Introduction

Despite their rarity, hot massive stars are prominent contributors to the dynamics and energetics of the ISM and to the global evolution of their host galaxies. The optical spectra of distant, star-forming galaxies exhibit numerous features typical of the UV spectra of O and B stars (Conti et al. 1996; Steidel et al. 1996). In order to determine the properties of starbursts galaxies at high redshift, it is thus essential to understand the physical properties

and evolution of massive stars in a low metallicity environment. O stars in the Small Magellanic Cloud offer the best opportunity to achieve this goal. Indeed, the SMC is a galaxy which is little evolved having a relatively low metal content, and is sufficiently close to obtain high-quality UV and optical spectra of individual stars. Additionally, modeling tools to analyze the photosphere and winds of hot, massive stars with a high level of accuracy and reliability have become available in recent years. Major progress has been achieved to model the stellar photosphere and stellar wind in an unified approach, as well as to incorporate a sophisticated treatment of NLTE line blanketing that accounts for all the important opacity sources in the stellar atmospheres (e.g., programs CMFGEN, Hillier & Miller 1998; WM-BASIC, Pauldrach et al. 2001; TLUSTY, Hubeny & Lanz 1995).

Winds from massive stars are radiatively driven through the transfer of momentum from the stellar radiation field to the atmospheric material via photon absorptions and scattering due to thousands of metal lines (Castor et al. 1975; Kudritzki & Puls 2000). An immediate consequence of the nature of these winds is that the wind properties (mass loss rate, terminal velocity) depend on the stellar metallicity. For example, Vink et al. (2001) have predicted that the mass loss rate scales as $\dot{M} \propto Z^{0.85}$, for metallicities ranging from 1/30 to 3 times the solar metallicity. The agreement between their predicted values and the measured mass loss rates for samples of O-type stars in the Milky Way is good (Vink et al. 2000), but they do not agree well for LMC stars and a large scatter is found for SMC stars (Vink et al. 2001). In this context, it is of special interest to derive accurate estimates of both elemental abundances and mass loss rates from the analysis of individual O stars in the SMC, in order to provide an important scaling law for evolutionary models of massive stars. Additionally, such analyses yield the quantities to further test the Wind-momentum Luminosity Relation (Puls et al. 1996) in a low metallicity environment.

Following the pioneering studies of SMC OB stars in the UV based on low resolution and limited signal-to-noise ratio data recorded by *IUE* (Smith-Neubig & Bruhweiler 1997) or HST/FOS (Walborn et al. 1995; Puls et al. 1996; Haser et al. 1998), Lennon led a spectroscopic survey of a score of SMC OB stars at higher spectral resolution in the UV with HST/STIS (Walborn et al. 2000). About half of the stars are located in NGC 346, the largest H II region in the SMC which has been extensively observed with ground-based telescopes in the past (Walborn 1978; Walborn & Blades 1986; Niemela et al. 1986; Massey et al. 1989). These new observations in the UV have been supplemented by optical spectroscopy.

Taking advantage of these new, high-quality spectroscopic data, Hillier et al. (2003) focussed their interest on describing the wind properties of O stars. They performed a detailed study of two stars, AV 83 and AV 69, which have similar effective temperatures, luminosities and metallicities, but show very different wind signatures. Their analysis indicates that the

O7 Iaf+ star AV 83 has a slow, dense wind, which most likely is highly clumped. Moreover, AV 83 reveals a substantial enhancement of its nitrogen surface abundance, consistent with the presence at the surface of material processed internally by the CNO cycle. On the other hand, the OC7.5 III((f)) star AV 69 has a substantially less dense wind and has a surface composition similar to SMC gas. These results are consistent with our current understanding of stellar evolution (e.g. Maeder & Meynet 2000) if AV 83 is a fast rotator which has experienced rotationally enhanced mass loss and rotationally induced mixing. On the other hand, AV 69 would be a slow rotator. Hillier et al. (2003) have systematically examined the influence of various parameters on the predicted spectrum, providing thus a solid basis for further studies of O star winds.

We present in this paper the result of our spectroscopic analysis, from the far-UV to the visible, of six O dwarf stars in NGC 346. We describe the observations and data reduction in Sect. 2. Section 3 discusses the model atmospheres used in our analysis, while the methodology used to derive the stellar parameters, chemical abundances, and winds parameters is exposed in § 4. We discuss our results and related uncertainties, star by star in Sect. 5. We put then our results in a broader astrophysical context in Sect. 6, comparing in particular the derived mass loss rates to theoretical predictions and discussing their dependence with the stellar metallicity. The paper closes on general conclusions (§ 7) based on this analysis of O dwarfs in the SMC low metallicity environment.

2. Observational Background

High-resolution, high-quality UV and optical spectra of a score of O stars in the SMC have been recorded to serve as a spectral template of a young stellar population in a low metallicity environment. A full description of the whole dataset and data reduction can be found in Walborn et al. (2000). The sample was selected with a bias towards stars with a sharp-lined spectrum, thus towards stars viewed preferentially pole-on or possibly towards intrinsically slow rotators. In this paper, we are concerned with six stars in NGC 346 that are on the main sequence. We only recall here the major characteristics and some relevant information about the selected stars. Table 1 summarizes the observational parameters of the stellar sample. Stars' identification (MPG number) is from Massey et al. (1989); spectral types and the photometry are taken from Walborn et al. (2000). Following Walborn et al. (2002), the hottest star of our sample, NGC 346 MPG 355, belongs to the newly-defined O2 spectral class and has been classified O2 III (f*). Formally, it is not an O dwarf, but dwarf and giant stars occupy nearly the same location in the HR diagram at the hot end of the main sequence. The inclusion of this star in our sample allows us to sample a range from

the earliest to the latest O stars. The spectral type of NGC 346 MPG 487 was attributed by Walborn (priv. comm.) based on the new visual spectroscopy discussed below. Radial velocities have been measured by shifting the observed spectra relative to the model spectra. Our radial velocities are very close to the values listed by Walborn et al. (2000).

2.1. UV Spectroscopy

Ultraviolet spectra have been obtained in the framework of *HST* General Observer program 7437 (PI: D. J. Lennon) for 19 O-type stars in the SMC. All program stars have been observed with STIS and the far-UV MAMA detector in the E140M mode, through the $0\farcs2\times0\farcs2$ aperture. A spectral interval from 1150 to 1700 Å is covered in a single exposure, at an effective resolving power, $R = 46\,000$. The STIS data have been reduced at Goddard Space Flight Center, using the CALSTIS software developed by the STIS Investigation Definition Team (Lindler 1999). Walborn et al. (2000) have described the reduction process in detail. The spectra are then normalized, because the predicted flux distribution in the far-UV not only depends on the assumed SMC distance but is very sensitive to the adopted correction of interstellar extinction.

2.2. Optical Spectroscopy

Complementary optical spectroscopy was obtained for all program stars (Walborn et al. 2000). Spectra of four stars of this sample (NGC 346 MPG 355, NGC 346 MPG 324, NGC 346 MPG 368, NGC 346 MPG 487) have been obtained at Anglo-Australian Telescope (AAT) with the echelle spectrograph UCLES. The spectral interval ranges from 3847 to 5008 Å, at a typical resolution, $R = 25\,000$. The seeing varied between $0\farcs8$ and $2''$. Additional observations of the red spectrum have been obtained to constrain the mass loss rate with Hα using the same instrumentation at a similar resolution. Observations of Hα have been secured for the three stars of our sample that show marked UV spectral signatures of a stellar wind (MPG 355, 324, 368).

The two other stars, NGC 346 MPG 113, and NGC 346 MPG 12, were observed with ESO 3.6 m telescope equipped with CASPEC. The spectra cover an interval from 3910 to 5170 Å, at a similar spectral resolution, $R = 25\,000$.

The echelle spectral data were reduced uniformly with the FIGARO package by the UCL group. Details on the procedure can be found in Walborn et al. (2000).

3. Models and Assumptions

Strong stellar winds, significant departures from the Local Thermodynamic Equilibrium (LTE) and an effect of numerous metal lines, traditionally called metal line blanketing, present the major difficulties in modeling the atmospheres of O-type stars. These three issues must be addressed by the model atmospheres in order to provide reliable photospheric and wind parameters of massive stars. This involves constructing fully-blanketed, NLTE models for an entire stellar atmosphere, going from a quasi-static photosphere out to the supersonic wind. Considerable advances in modeling techniques have been achieved during recent years (for a number of recent reviews, see Hubeny et al. 2003), and several computer programs that can handle this problem are available now – program CMFGEN (Hillier & Miller 1998); PHOENIX (Hauschildt et al. 1997); Munich programs (Pauldrach et al. 2001); and the Kiel-Potsdam code (Koesterke et al. 2002).

Unified models, with a consistent treatment of the photosphere and the wind, are obviously necessary to analyze the P Cygni profile of strong lines in the UV spectra of O stars and then derive the basic wind parameters (mass loss rate, terminal velocity). However, hydrostatic, fully-blanketed, NLTE photospheric models may in many cases remain a preferable alternative to unified models with a simplified treatment of a photosphere. Indeed, the bulk of spectral lines in O stars are formed in the photosphere where velocities are small and geometrical extension is negligible. The spectrum of slowly-rotating O stars show mostly narrow and symmetric lines (see, e.g., NGC 346 MPG 113, Fig. 7). This statement is valid in all but the most extreme cases of stellar winds, like those observed in Wolf-Rayet stars and extreme Of supergiants. Moreover, winds are weaker in low-metallicity environments making photospheric models even more relevant in this case. Additionally, there are many remaining uncertainties as to the exact properties of stellar winds of hot stars, even though the paradigm of radiatively-driven winds is well established. For example, we do not have in many cases a consistent solution: the calculated line force is often too small to drive a wind through the critical point (though some progress is being made), so a β-type velocity law must be adopted to describe empirically the velocity and density structure of the wind. While mathematically trivial, it is physically not so obvious how to connect the photospheric exponential density structure with the wind power law (see Hillier et al. 2003 for a discussion); some spectral features are formed in the connection region. Furthermore, radiative equilibrium is not really satisfied in these winds, where shocks dump mechanical energy and heat the wind, thus changing its ionization structure (e.g., super-ionization). Finally, the assumption of one-dimensional geometry is challenged by the likely presence of dense clumps in the wind and by rotation; the role of magnetic fields is not yet understood, and their importance in structuring the wind will very likely be more important than in the photosphere.

Therefore, we have performed an analysis using model atmospheres calculated with the photospheric program, TLUSTY, and the unified model code, CMFGEN. We intend to compare the parameters derived from these two NLTE model atmosphere programs; we may consider them as two independent programs although the atomic data used by the two codes come mostly from the same sources. Second, we will examine the effect of an extended stellar wind on the photospheric lines in O dwarf spectra. We describe thereafter the basic characteristics of these two codes.

3.1. Photospheric Models

Photospheric models have been constructed with the model atmosphere code, TLUSTY (Hubeny & Lanz 1995). The main assumptions of the code are a plane-parallel geometry, hydrostatic equilibrium, and radiative equilibrium. Departures from LTE are explicitly allowed for a large set of chemical species and arbitrarily complex model atoms. Line opacity is treated in detail using an Opacity Sampling technique with close to 200 000 frequency points over the whole spectrum. For this work, we have extracted models from the new, extensive OSTAR2002 grid (Lanz & Hubeny 2003b). These fully-blanketed, NLTE model atmospheres include about 100 000 individual atomic levels from 45 ions (H I-II, He I-III, C II-V, N II-VI, O II-VII, Ne II-V, Si III-V, P IV-VI, S III-VII, Fe III-VII, Ni III-VII), as summarized in Table 2. We have selected models with a scaled-solar composition, $Z/Z_\odot =$ 1/5, and 1/10, that are appropriate for SMC stars. We have adopted the solar abundances from Grevesse & Sauval (1998). All model atmospheres assume an helium abundance, $y =$ He/H = 0.1 by number[9], and a microturbulent velocity, $\xi_t = 10\,\mathrm{km\,s^{-1}}$. The OSTAR2002 model atmospheres are described in detail by Lanz & Hubeny (2003b).

Lanz & Hubeny (2003b) have pointed out that the omission of highly-excited atomic levels of light species in OSTAR2002 model atmospheres results in underestimating some recombination rates. We have therefore recalculated a limited number of model atmospheres with more extensive model atoms for C III and N IV in order to achieve a better prediction of recombination lines seen in emission in the visible spectrum.

TLUSTY solves for the full photospheric structure, providing the temperature and density stratification and the NLTE populations. A detailed synthetic spectrum is then calculated with SYNSPEC, varying if necessary the abundance of individual species (e.g., the N/C abundance ratio), or the microturbulent velocity. However, we have always imposed the condition that the photospheric turbulent velocity remains smaller than the photospheric

[9]Throughout this paper, chemical abundances are quoted by number density relative to hydrogen.

speed of sound (typically, $c_{\rm sound} \leq 25\,{\rm km\,s^{-1}}$).

3.2. Wind Models

Spherically symmetric wind models have been constructed with the NLTE code CMFGEN (Hillier & Miller 1998; Hillier 2003). This code solves the radiative transfer equation in the co-moving frame, together with statistical equilibrium equations. The wind models include 28 explicit ions of H, He, C, N, O, Ne, Si, P, S, and Fe. A total of 3300 individual levels grouped into 900 superlevels are included, with a full array of over 20 000 bound-bound transitions. The ionization stages, number of individual levels and superlevels of each model atom are summarized in Table 2. We have adopted an atomic data set that is consistent with the data set used by Hillier et al. (2003). Radiative equilibrium has been assumed to determine the temperature structure throughout the atmosphere.

CMFGEN does not solve the momentum equation, and a density or velocity structure is therefore required beforehand. The velocity in the stellar wind is parameterized with a classical β-type law which is connected to an hydrostatic density structure at depth. We have taken the hydrostatic structure from TLUSTY models. At the connecting point, we require that the velocity and the velocity gradient both match. O star model spectra are relatively sensitive to the exact density structure which is assumed around the sonic point if the wind is dense enough. Hillier et al. (2003) have presented a detailed discussion of this issue for AV 83. Since few lines show evidence of a wind in our stellar sample, this problem is likely not as severe as in AV83 and most diagnostic lines should be insensitive to it.

We have assumed a depth-independent Doppler profile for all lines when solving for the atmospheric structure in the co-moving frame. Martins et al. (2002) have shown that the resulting atmospheric structure, level populations, and emergent spectrum, is not changed by this approximation. In this step, we used the microturbulent velocity, $\xi_{\rm t}^{\rm phot}$, derived from TLUSTY analysis. In the final calculation of the emergent spectrum in the observer's frame, we have however adopted a radially-dependent turbulence, expressed as

$$\xi_{\rm t}(r) = \xi_{\rm t}^{\rm phot} + (\xi_{\rm t}^{\rm max} - \xi_{\rm t}^{\rm phot})\frac{v(r)}{v_\infty}, \qquad (1)$$

where $v(r)$ and v_∞ are the velocity law and the terminal velocity of the wind, and $\xi_{\rm t}^{\rm max}$ is the maximum turbulent velocity (see § 4.4). Such a turbulent velocity law reflects the effect of shocks due to wind instabilities. Moreover, we have taken into account incoherent electron scattering and Stark broadening for H I, He I, He II lines.

CMFGEN can account for clumping in the stellar wind which results from the unstable

nature of radiatively-driven winds. Clumping is described assuming a volume filling factor, f, that there is no interclump medium, and that the clumps are small compared to the mean free path of photons. The filling factor is parameterized following an exponential decrease

$$f = f_\infty + (1 - f_\infty) \exp(v/v_{\rm cl}), \tag{2}$$

where $v_{\rm cl}$ is the velocity at which clumping starts. We have assumed that clumping starts at $v_{\rm cl} = 30\,{\rm km\,s^{-1}}$, just above the sonic point. The detailed implementation of clumping in CMFGEN is discussed by Hillier (1997) and by Hillier & Miller (1998).

4. Methodology

We start the analysis using TLUSTY OSTAR2002 models (Lanz & Hubeny 2003b). The photospheric parameters derived from this analysis provide the initial values for a second analysis with the unified, wind code, CMFGEN. In this second step, we still allow for changes in the photospheric parameters, because CMFGEN models also have a realistic description of photospheric layers. We then compare the consistency of the two analyses.

4.1. Determination of Photospheric Parameters

Following a long-established way to analyze O star spectra, we first attempt to match the Balmer H I, He I and He II lines between 3800 and 5000 Å to determine initial estimates of the photospheric parameters ($T_{\rm eff}$, $\log g$, y = H/He). The He I to He II line strength ratios are the characteristic $T_{\rm eff}$ indicator in main-sequence O stars, while $\log g$ is constrained from Balmer line wings. A simultaneous fit of all optical lines of these ions proves however often elusive. The task is further complicated by a nebular contamination of the Balmer and He I lines since NGC 346 is embedded in strong nebulosity. Our initial $T_{\rm eff}$ diagnostics lines are thus He I λ4388, 4471, 4713, 4922, and He II λ4200, 4541, 4686. The latter He II line is often affected by a stellar wind, leading several authors to disregard He II λ4686 as a $T_{\rm eff}$ indicator (e.g. Crowther et al. 2002). However, the stellar wind of SMC O dwarfs is weak enough (see § 5) that this line may be helpful. We have not used specifically He II λ1640. On one hand, this line does not provide additional photospheric diagnostics. On the other hand, we have not observed in our stellar sample much influence of the stellar wind on this line, mostly because the winds are not dense enough.

In addition to the optical spectrum, we also rely on ionization balance of heavy elements in the UV spectrum. We need however to disentangle their temperature sensitivity from other parameters, *(i)* the microturbulent velocity (e.g O IV λ1338-43, S V λ1502, Fe IV-VI

lines), *(ii)* the mass loss rate (O IV λ1338-43, O V λ1371, C III λ1176), not to mention *(iii)* the adopted chemical abundances. The OSTAR2002 grid allows us to study trends and to define the best strategy. The safest approach in limiting the role of other parameters consists in considering line ratios of two (or more) successive ionization stages of a given chemical element. Therefore, we have mostly used the C III λ1176 to C IV λ1169 ratio and iron ions as primary temperature diagnostics (see also Heap et al. 2003a). Comparisons between photospheric (TLUSTY) and wind (CMFGEN) models have also helped to estimate the effect of the stellar wind on temperature sensitive lines; specific results are discussed in § 5. The $T_{\rm eff}$ accuracy is typically of the order of several percent.

Usual spectroscopic diagnostics of $\log g$ are Balmer line wings, most especially Hγ. High accuracy determinations of $\log g$ which are required to derive accurate stellar masses are difficult to achieve. Indeed, the line wings change relatively little compared to observational limitations (nebular emission; spectra with moderate signal-to-noise ratios). Moreover, a strong stellar wind fills the Balmer lines and thus results in underestimating the surface gravity (Sellmaier et al. 1993; Schaerer & Schmutz 1994). This later problem should however remain limited with weaker winds in low metallicity environments. We have thus always checked our initial estimates derived from TLUSTY models with CMFGEN fits to Balmer lines. We stress finally that the *effective gravity* of the models is significantly lower than the real gravity because of the influence of the radiation pressure (see Fig. 3 in Lanz & Hubeny 2003b). The influence of centrifugal acceleration is however ignored, and hence the actual gravity is underestimated, particularly for fast stellar rotation.

A simultaneous fit of all He I and He II lines is almost never achieved (see, e.g., Herrero et al. 1992; Hillier et al. 2003), leaving significant uncertainties on helium abundance determinations. Earlier studies systematically found enhanced helium abundances (Herrero et al. 1992), while standard stellar evolution models (without rotation) do not predict such a surface enrichment for main-sequence O stars (Maeder 1987a). Smith & Howarth (1998) showed that consistent fits of the helium lines in O supergiants can be achieved when introducing a microturbulent velocity, helping to solve the "helium discrepancy" problem (Herrero et al. 1992). In this study, we have adopted an helium abundance, $y = 0.1$, as in TLUSTY OSTAR2002 grid, and we start the analysis assuming a microturbulent velocity, $\xi_{\rm t} = 10\,{\rm km\,s^{-1}}$. There is no indication of helium enrichment in our stellar sample.

4.2. Stellar Luminosities and Radii

Absolute visual magnitudes were calculated from the photometry in Table 1, assuming a distance modulus of 19.1 mag (i.e., a distance of 66.1 kpc) for the SMC following Walborn

et al. (2000). Our absolute magnitudes are slightly smaller than Walborn, et al.'s (2000) due to lower extinction derived from OSTAR2002 theoretical intrinsic colors (typically, our color excesses are 0.02 mag smaller). The stellar luminosities were then obtained applying a bolometric correction from Lanz & Hubeny (2003b). This OSTAR2002 relation, BC *vs.* $T_{\rm eff}$, is very similar to the de Koter et al. (1998) relation and to the empirical relation of Chlebowski & Garmany (1991). The derivation of stellar radii is then straightforward.

4.3. Microturbulent Velocity and Chemical Abundances

We have used OSTAR2002 model atmospheres with $Z/Z_{\odot}$= 1/5, and 1/10, to determine the stellar metallicities, fitting the numerous iron lines in the UV spectrum. Departures from scaled-solar abundances have been considered for carbon and nitrogen. We have recomputed model spectra with SYNSPEC and CMFGEN assuming different C and N abundances. Oxygen abundances cannot be derived reliably from our spectra: O IV λ1338-43 strength is very sensitive to the adopted microturbulent velocity, and O V λ1371 is formed in the stellar wind. Similarly to the O IV lines, S V λ1502 is mostly useful to derive $\xi_{\rm t}$. We kept abundance ratios fixed to the same scaled-solar value for all other species included in the model atmospheres (O, Ne, Si, P, S).

4.4. Wind parameters

After the photospheric analysis, the parameter space left to explore is greatly reduced. Using CMFGEN, we derive in the next step the wind parameters (namely, $\dot{M}$, v_{∞} and β) keeping $T_{\rm eff}$ within the error bars of the photospheric analysis. Our analysis assumes an homogeneous wind and neglects clumping in the wind at the present stage. We will however comment further on this point in § 6.

Initial estimates of the mass loss rates have been calculated with a theoretical formula from Vink et al. (2001). The mass loss rates are adjusted until we match the observed spectra. The three stars with earlier spectral type exhibit P Cygni line profiles in the UV spectrum. The primary diagnostic lines available to determine the mass loss rate are the C IV resonance doublet, the N V resonance doublet, and O V λ1371. The N V lines are sensitive to the presence of shocks in the wind and a match to the O V line is often difficult to achieve. Other potentially useful UV features are C III λ1176, O IV λ1338-43, He II λ1640, and N IV λ1718. In the optical, we have recorded spectra around Hα for these three stars. In all cases, Hα is an absorption line which does not significantly depart from a

pure photospheric profile. Hα and other UV lines help nevertheless to set limits on the mass loss rate. The spectrum of the three stars with a later spectral type, NGC 346-113, NGC 346-487, and NGC 346-12, do not reveal any P Cygni line profiles, but only weak blue-shifted absorption in C IV and N V resonance lines. We could then only establish upper limits on the mass-loss rate.

Simultaneously, we have to determine the exponent β of the wind's velocity law. The predicted line profiles are quite sensitive to the density in the sonic region and thus depend on the adopted β. For weak stellar winds, there is often a degeneracy in the determination of $\dot{M}$ and β (see also Hillier et al. 2003). We have adopted $\beta = 1$ as the default value, but we have still explored cases of slightly different β, $0.7 \leq \beta \leq 1.5$.

Apart from N V λ1240 in MPG 355, our spectra do not reveal any saturated P Cygni lines to measure the wind terminal velocity, v_∞. Following Prinja & Crowther (1998), we have thus used narrow absorption components seen in MPG 324 and in MPG 368 spectra to determine v_∞. We can only derive lower limits of the wind terminal velocity for the three other stars. The maximum turbulent velocity in the wind (Eq. 1) is derived by fitting the blue edges of the P Cygni line profiles, while the minimum value has been set from the photospheric analysis. Turbulence in the wind affects little the ionization structure of the models, and is only necessary to achieve a match to the observed profiles.

We have adopted in a first step homogeneous wind models, but we have been unable to match some of the line profiles (most notably, O V λ1371, see §5). We have therefore examined the influence of clumping in a second stage.

4.5. Projected Rotational Velocities

TLUSTY spectra are convolved with a rotational profile and a Gaussian instrumental profile in order to compare them with observed spectra. The projected rotational velocity $V \sin i$ is derived by matching relatively weak iron lines, as well as C III λ1176, O IV λ1338-43, and S V λ1502. The C III λ1176 multiplet is very useful because of its 6 close line components. In the STIS spectra, all stars but NGC 346-355 (too hot to show strong C III lines) show partial or fully resolved multiplet components, indicating moderate ($V \sin i < 100\,\mathrm{km\,s^{-1}}$) to slow ($V \sin i \approx 20\,\mathrm{km\,s^{-1}}$) rotational velocities. The projected rotational velocities are determined with a typical precision of $\pm 10\,\mathrm{km\,s^{-1}}$.

Limited work exist so far on rotating stellar winds, because an exact calculation of line profiles formed in an extended wind requires multi-dimensional model atmospheres (see, e.g., Petrenz & Puls 1996). Convolution with an analytical profile is a reasonable approximation

for photospheric lines only, as long as the rotational velocity does not approach the break-up velocity. In our case, most lines are formed in the quasi-static photosphere or in the sonic region since the wind is relatively weak (very few lines even show a P Cygni profile). Moreover, rotational velocities remain small as indicated by the C III λ1176 multiplet. We believe therefore that we may apply a rotational convolution to observer's frame spectra calculated with CMFGEN with a relative safety.

4.6. Interstellar Absorption Lines

The UV spectra reveal two sets of narrow interstellar absorption lines, from Galactic and SMC gas. A detailed modeling of these features is left to a future paper. However, we have added Lyα interstellar contribution to the theoretical spectra, in order to compare observed and predicted spectral features near Lyα (e.g., Si III λ1206, N V λ1240). We have varied the H I column until a match to the observed Lyα profile is achieved.

5. Results of the Spectroscopic Analysis

We discuss in this section the properties, the results and uncertainties of the analysis of each individual star. A general discussion about the sample as a whole, of the astrophysical significance of the results, and a comparison to theoretical predictions is left to the next section.

5.1. NGC 346 MPG 355

This star has long been classified as an O3 III ((f*)) star (Massey et al. 1989; Walborn et al. 2000), based on the absence of He I λ4471 in its spectrum. Recently, Walborn et al. (2002) have reexamined the earliest O-type stars and have introduced two new spectral classes, O2 and O3.5, to distinguish stars having no or very weak He I λ4471, but different N III-V lines. MPG 355 exhibits N V λ4603-19 in absorption, strong N IV λ4058 in emission, and no N III λ4640. This star belongs thus to the newly defined O2 class, and is classified O2 III (f*). Taresch et al. (1997) used similarly the nitrogen ionization balance to derive the effective temperature of the O3If star, HD 93129A.

Haser et al. (1998) have analyzed a low resolution (7 Å) HST/FOS spectrum of MPG 355. We compare their findings to our new results based on higher resolution spectra recorded with HST/STIS.

The spectral type, the helium and nitrogen lines indicate that this star is unusually hot. We found that a TLUSTY model atmosphere with $T_{\rm eff}$= 52 500 K, $\log g$=4.0, and a metallicity 1/5 the solar value, provides the best match to the observations. This model atmosphere reproduces also well the Fe IV-VI line strength ratios in the UV. The C III λ1176 lines are very weak and can only be used to set a lower limit to $T_{\rm eff}$. A slightly lower effective temperature, $T_{\rm eff} \approx 50\,000$ K, is favored by S V λ1502, while the fit to He II λ1640, 4686 is improved at higher $T_{\rm eff}$ (54-55,000 K). We estimate the uncertainties to be $\pm$2500 K and $\pm$0.1 dex on $T_{\rm eff}$ and $\log g$, respectively. Within the quoted uncertainties, our results agree with Haser et al. (1998) values.

Simultaneously, we have derived a microturbulent velocity, $\xi_{\rm t}$=25 km s^{-1}, from a fit to S V λ1502, while assuming a sulfur abundance, S/S$_\odot$=0.2. The O IV λ1338-43 and the Fe lines are also well matched with this microturbulent velocity, assuming 1/5 times the solar abundances. The Fe lines can alternatively be matched with a lower abundance, one tenth of the solar value, while increasing the turbulent velocity to a supersonic value ($\xi_{\rm t} \approx 35$ km s^{-1}); however, the fit to other lines, e.g. C IV λ1169 or S V λ1502, is lost. A microturbulent velocity as large as 25 km s^{-1} is of similar order than the photospheric sound speed in MPG 355. Although a quite large value, it is unlikely that this is a spurious result. Indeed, such large microturbulence is required to match lines of different species and is therefore not a result of shortcomings of the adopted model atoms. Furthermore, CMFGEN models also require a microturbulent velocity of the same order to match the observed spectrum. This microturbulence mimics non-thermal motions in the atmosphere. Results from CMFGEN models show that this large microturbulence is not a spurious artefact of static model atmospheres which neglect the desaturation of spectral lines by a macroscopic velocity field – the stellar wind, as was suggested by Kudritzki (1992). Denser winds are necessary for the latter to become effective (i.e. lines need to be formed in the sonic region, but they will then show a blue asymmetry).

A match to the observations is achieved after including a rotational convolution, with $V \sin i$=110 km s^{-1}.

In the ultraviolet, the carbon abundance can only be determined by fitting C IV λ1169. Only an upper limit can be set with C III λ1176, while the C IV λ1549 is formed in the wind and its strength depends on the adopted mass loss rate and other wind parameters. A carbon abundance, C/C$_\odot$=0.2, provides a good match to C IV λ1169. The $3s - 3p$, C IV λ5801-12 lines are predicted in emission by this hot model atmosphere and are observed in emission. This doublet is well fitted with the adopted carbon abundance. Moreover, C IV λ5801-12 emission brings further support to our adopted effective temperature. TLUSTY OSTAR2002 models indeed predict that this doublet turns into emission at $T_{\rm eff} \geq 50\,000$ K, with stronger

emission at higher effective temperatures. At $T_{\rm eff} \leq 47\,500\,{\rm K}$, these lines are predicted in absorption.

From N IV λ4058 and N V λ4603-19, we have derived a solar nitrogen abundance, showing thus a significant nitrogen enrichment at the stellar surface. Even with this overabundance, the model predicts no visible N III λ4640, as observed. This nitrogen abundance also provides a good fit to N IV λ1718, while the N III λ1182-84 lines remain very weak. The N V resonance doublet cannot be used to determine a reliable abundance since the N V density in the wind might be strongly affected by shocks and the related X-ray emission.

Oxygen abundance cannot be derived reliably: O IV λ1338-43 lines are most sensitive to the adopted microturbulent velocity, while O V λ1371 is formed in the wind (see further discussion below). We have thus assumed by default a scaled-solar value comparable to the derived metallicity (1/5 solar).

Haser et al. (1998) have similarly found a stellar metallicity of 1/5 the solar metallicity, based on spectrum synthesis analysis of the low resolution HST/FOS spectrum and indirect hydrodynamical arguments. We stress however that our determination is more robust because the higher resolution of STIS allows us to disentangle the numerous line blends in the UV spectrum. We estimate that the accuracy of our abundance determinations is typically $\pm 0.2\,{\rm dex}$. Already from line strength consideration (N V λ1240 *vs.* C IV λ1549), Walborn et al. (1995, 2000) recognized that MPG 355 has a surface composition very likely enriched in nitrogen, which was confirmed by Haser et al. analysis. Our results indicate an even larger nitrogen enrichment. On the other hand, Haser et al. found a very low carbon abundance, $C/C_{\odot}$=0.02, claiming even that this value had to be an upper limit. This result was based on the C IV λ1549 resonance doublet, for which Haser et al. estimated a contribution from shocks in the wind. They were unable to find any consistent solution for several wind lines without adopting this very low carbon abundance. The C IV λ1169 line in our STIS spectrum cannot be reconciled at all with Haser et al. low carbon abundance.

Fig. 1 displays the best TLUSTY and CMFGEN model fits to these lines formed in the "quasi-static" photosphere.

Using the parameters and abundances derived with TLUSTY, we have then constructed a number of wind models with CMFGEN. We achieve a good agreement between TLUSTY and CMFGEN models for lines of weak and moderate strength formed in the pseudo-photosphere. Wind parameters are derived from the strongest lines. The terminal velocity and maximum turbulent velocity in the wind are set from the only saturated lines, N V λ1240. We have adopted a terminal velocity, v_{∞}= $2800\,{\rm km\,s^{-1}}$, and a maximum turbulent velocity in the wind of $160\,{\rm km\,s^{-1}}$. The mass loss rate and wind acceleration parameter, β, are derived by

fitting C IV λ1549 and Hα. We found a mass loss rate, $\dot{M}= 2.5\,10^{-6}\,M_\odot\,yr^{-1}$, for a wind without clumps, and $\beta = 0.8$, in order to reproduce C IV emission without filling the Hα core too much. We can exclude slow acceleration winds, $\beta \geq 1.5$, for which we cannot achieve a consistent fit of C IV λ1549 and Hα, given the adopted carbon abundance. Emission due to incoherent electron scattering in the wings of He II λ1640, 4686[10] is predicted somewhat too strong. A higher effective temperature (55 000 K) would solve this problem.

N V λ1240 is also predicted somewhat too strong. Furthermore, our wind model does not reproduce well the observed asymmetry of N IV λ1718 (extended blue absorption), contrary to the case of the cooler stars, MPG 324 and MPG 368. Our adopted wind model predicts thus too high a nitrogen ionization in the wind of MPG 355. On the other hand, the photospheric N IV/N V ionization balance reproduces well the lines in the blue spectrum. The theoretical soft X-ray flux ($\lambda < 160$ Å, N IV ionization edge) is of correct order in the photosphere and in the sonic region but is still too strong in the wind, even though we have neglected the possible influence of shocks. We note that Haser et al. (1998) similarly predicted N V λ1240 too strong.

O V λ1371 reveals a problem encountered in all previous analyses of O stars that show O V λ1371: the model wind atmospheres predict too strong absorption at moderate velocities, too little absorption at low velocities, and too strong emission. We have thus examined the influence of clumping on this line. We have calculated several models with different clump volume filling factors, adjusting the mass loss rate so that we keep a good fit to C IV λ1549. Hα core is somewhat filled by wind emission and provides a further constraint on the mass loss rate. Fig. 2 shows that we can achieve a good match of O V λ1371 when assuming a very small filling factor, $f_\infty = 0.01$, with a mass loss rate, $\dot{M}= 1.8\,10^{-7}\,M_\odot\,yr^{-1}$. A larger filling factor, $f_\infty = 0.1$, and a lower oxygen abundance (by a factor 4) does not fit the observed profile as well as the very small f_∞ though it already improves over the case of homogeneous winds. Although the larger clumping factor seems more reasonable and the O IV λ1338-41 lines are still matched with the lower abundance (these lines are saturated and are thus quite insensitive to changes in abundance), we do not find any compelling argument to adopt an oxygen abundance a factor 3 lower than the nebular abundance while carbon is not depleted as well (as carbon depeletion is expected first for CNO-cycle processed material). The sharp transition between the absorption and emission components indicates that clumps start forming at low velocities, $v \approx 30\,km\,s^{-1}$, just above the sonic point. The other wind line profiles are little changed relative to profiles predicted by an homogeneous wind model.

[10]The extent of He II λ4686 wings remains ill-defined due to difficulties in defining an "exact" continuum in the echelle spectrum.

We have explored a number of other possibilities in order to reproduce O V λ1371. The key point consists in predicting the correct O IV/O V ionization structure in the vicinity of the sonic point. To alter ionization, we have considered X-ray emission from shocks in the wind ($L_X/L_{\rm bol} = 2\,10^{-7}$), adiabatic cooling, larger model atoms, and alternate recombination rates (Nahar 1999). All these changes resulted in essentially no difference in the synthetic spectrum.

Alternatively, de Koter et al. (1998) argued that O3 stars are cooler (40 000 K $\leq T_{\rm eff}$ $\leq$ 46 000 K), based on the O IV/O V line strength ratio. These low temperatures are not supported by our other $T_{\rm eff}$ estimators. Moreover, the mismatch of the O V λ1371 line is still qualitatively the same, revealing a problem with the wind models at low and moderate velocities where the validity of the Sobolev approximation (assumed by de Koter's ISA-WIND program) is not established. We stress however that the critical issue is clumping, and not the Sobolev approximation, as demonstrated by the failure of homogeneous wind models (see Fig. 2, and also Fig. 9 in Haser et al.) to reproduce the observed line profile.

A full examination of the far-UV spectrum and of the visible spectrum reveals that only few other lines are influenced by the stellar wind, even for a star with such an early spectral type and a moderate wind ($\dot{M} \approx$ few $10^{-6}\,{\rm M}_\odot\,{\rm yr}^{-1}$). These lines include O IV λ1338-43, N IV λ1718, and few strong Fe lines, whose cores are filled a little by wind emission. Otherwise, we have a very good consistency between TLUSTY and CMFGEN model spectra. This agreement shows that we can use NLTE photospheric models to derive stellar parameters and abundances, even for the hottest O dwarfs with moderate winds.

5.2. NGC 346 MPG 324

We are able to match the Balmer line series and the He II lines with a TLUSTY model atmosphere, assuming $T_{\rm eff} = 40\,000$ K and $\log g = 4.0$. On the other hand, the He I lines are virtually absent which suggests an effective temperature of about 45 000 K. However, the visible spectrum is contaminated with nebular emission, suggesting that the weakness of the He I lines is mostly due to line filling by this emission. Walborn et al. (2002) showed that the different ionization stages of nitrogen can be used as a temperature indicator, but the nitrogen lines are hardly seen in the visible spectrum of MPG 324 and therefore cannot be used for this purpose. Based on the visible spectrum only, our estimates support earlier results from Puls et al. (1996), who found $T_{\rm eff} = 40\,000$ K and $\log g = 3.7$.

The UV spectrum provides additional temperature criteria and TLUSTY and CMFGEN model atmospheres lead to exclude the higher temperatures suggested by the weakness of the

He I lines. Using the C III to C IV and the Fe IV/Fe V/Fe VI ionization balances, our analysis yields a best overall match when adopting $T_{\rm eff} = 41\,500\,{\rm K}$ and $\log g = 4.0$. Uncertainties are estimated at $\pm 2\,000\,{\rm K}$ in temperature and ± 0.1 dex in gravity. We achieve consistent results between the UV and visible spectra, as well as between TLUSTY and CMFGEN models. Fig. 3 displays the best fits to photospheric lines.

We have derived a moderate apparent rotational velocity, $V \sin i = 70\,{\rm km\,s^{-1}}$, from the partly resolved line structure of the C III λ1176 multiplet. This is slightly lower than a previous estimate listed by Walborn et al. (2000). We then fix the microturbulence velocity, $\xi_{\rm t} = 15\,{\rm km\,s^{-1}}$, by matching O IV, S V, and Fe lines, assuming a scaled-solar model with $Z/Z_\odot = 0.2$. Alternatively, we can adopt a higher microturbulence velocity, $\xi_{\rm t} = 20\,{\rm km\,s^{-1}}$, and a lower metallicity, $Z/Z_\odot = 0.1$. The latter fit is not as good, but provides an estimate of the typical uncertainty on abundances. Although we cannot derive oxygen and sulfur abundances independently to the microturbulence value, we have examined the case of a lower oxygen abundance because the adopted abundance, $O/O_\odot$=0.2, provides a poor fit to O V λ1371. We cannot reduce the oxygen abundance by much without increasing the microturbulent velocity to unrealistic values. Moreover, we remain unable to reproduce the O V λ1371 line with homogeneous wind models.

The carbon abundance was derived using TLUSTY and SYNSPEC models to fit simultaneously C III λ1175 and C IV λ1169, using the parameters previously derived. We have also constrained the carbon abundance from the absence of C III λ4647-51 in the visible spectrum (neither emission nor absorption). We found that the SMC nebular abundance, $C/C_\odot$=0.06 (Venn 1999), results in a good fit.

The nitrogen abundance, $N/N_\odot$=0.2, is derived from the N III λ1182-84 lines. The other nitrogen lines are not as sensitive as these lines to derive the nitrogen abundance. The N V resonance doublet is quite sensitive to the adopted wind parameters, the N IV λ1718 is only marginally sensitive to the abundance, while the lines in the visible spectrum are very weak given the signal-to-noise ratio of the data. While it might appear that the derived abundance remains subject to some uncertainty, we can exclude low abundances, $N/N_\odot < 0.1$, for which we cannot match the UV N IV and N V lines, as well as large abundances, $N/N_\odot > 0.5$ which would yield nitrogen emission lines in the visible.

From N V λ1240, we have measured a wind terminal velocity, $v_\infty = 2300\,{\rm km\,s^{-1}}$. This is in good agreement with a value derived from narrow absorption components. Therefore, even though the wind lines are not totally saturated, this value should likely not be much lower than the actual terminal velocity. The mass loss rate and the β exponent of the wind velocity law have been determined fitting the few available P Cygni profiles, in conjunction with other wind sensitive lines, like He II λ1640 or N IV λ1718 in the UV and Hα in the

visible. For an homogeneous wind, we find $\dot{M} = 2.7{\times}10^{-7}$ $M_\odot\,yr^{-1}$, and $\beta = 1.0$. Our estimate of the mass loss rate is consistent with an upper limit derived by Puls et al. (1996). The fits to the wind lines of MPG 324 are displayed in Fig. 4. Similarly to MPG 355, the homogeneous wind models fail to reproduce the O V λ1371 line profile. A much improved fit is achieved with a clumped wind model assuming a volume filling factor, $f_\infty = 0.1$, and a mass loss rate, $\dot{M} = 1.0{\times}10^{-7}$ $M_\odot\,yr^{-1}$.

5.3. NGC 346 MPG 368

As indicated by the spectral type, strong spectral similarities exist between MPG 368 and MPG 324. We have thus started our analysis of MPG 368 assuming MPG 324 stellar parameters and only minor changes were required to fit MPG 368 spectrum. We discuss our results in a comparative way to MPG 324; the same spectral regions are thus displayed in Fig. 5 and Fig. 6.

The analysis of the photospheric spectrum in the optical is hampered by strong H and He nebular emission, resulting in some uncertainty in deriving the effective temperature. However, like MPG 324, the carbon and iron ionization balances from UV lines allow us to derive reliably an effective temperature, $T_{\rm eff} = 40\,000$ K. Balmer line wings are slightly narrower than in MPG 324, resulting in a best fit for $\log g = 3.75$. The He II lines are not matched as well as in MPG 324 spectrum; the adopted model atmosphere yields too deep He II lines compared to the observed line profiles. O IV, S V, and Fe lines, are matched adopting the same microturbulent velocity, $\xi_{\rm t} = 15\,{\rm km\,s^{-1}}$, the same metallicity, $Z/Z_\odot = 0.2$, and a rotational velocity, $V \sin i = 60\,{\rm km\,s^{-1}}$.

The carbon abundance is derived in matching C III λ1176 and C IV λ1169. The models should also not predict strong C III λ4647-51 emission that is not observed. We find a carbon abundance, $C/C_\odot = 0.06$, that is consistent with the SMC nebular abundance, and similar to MPG 324 abundance. The nitrogen lines are clearly stronger in MPG 368 (e.g., N III λ1182-84, hint of an emission in N III λ4634-40), thus indicating that the surface of MPG 368 has been enriched in nitrogen. We have adopted, $N/N_\odot = 0.6$. The nitrogen enrichment of MPG 368 compared to MPG 324 is consistent with its being more evolved (indicated by a lower $\log g$) than MPG 324.

The wind lines of the two stars are also very similar, and we have derived with CMFGEN similar parameters. Consistent with the slightly lower effective temperature and luminosity, we have obtained a slightly lower mass loss rate, $\dot{M} = 1.5{\times}10^{-7}$ $M_\odot\,yr^{-1}$, lower terminal velocity, $v_\infty = 2100\,{\rm km\,s^{-1}}$, and $\beta = 1.0$. Abundances are the same than those adopted

from the photospheric analysis. The nitrogen enrichment results in a stronger asymmetry of N IV λ1718 compared to the case of MPG 324, and our final model reproduces well the extended blue absorption.

Like MPG 355 and MPG 324, we are able to fit O V λ1371 when allowing for clumps, while such a match cannot be achieved with homogeneous wind models. We achieve a best fit with a slightly lower volume filling factor, $f_\infty = 0.05$, and a mass loss rate, $\dot{M} = 5.7 \times 10^{-8}\,\mathrm{M_\odot\,yr^{-1}}$. The fit to N V λ1240 is also clearly better with the clumped wind model, though the emission is still predicted too strong without having yet accounted for the overionization due to shocks. The detailed profile of the N V lines may indicate that clumping follows a distribution that is more complicated than assumed, as suggested by the strong absorption component seen in MPG 324 and MPG 368 near terminal velocity.

5.4. NGC 346 MPG 113

This star has been classified as OC6 Vz by Walborn et al. (2000). They noted the presence of weak C III λ 4647-50 emission lines without N III λ 4634-40, indicating a low N/C abundance ratio. Furthermore, the large relative strength of He II λ 4686, the weak He I lines, and the extreme weakness of the UV wind lines, lead them to assign a Vz class to MPG 113 which suggests thus a very young age.

Our analysis yields an excellent match to the hydrogen and helium spectrum with the TLUSTY model, $(T_{\rm eff}, \log g) = (40\,000\,\mathrm{K}, 4.0)$. This model agrees also very well with the UV spectrum once we have fixed the turbulent microturbulent velocity, $\xi_{\rm t} = 10\,\mathrm{kms}$, with O IV and S V lines. The derived metallicity from the numerous UV lines is $Z/Z_\odot = 0.2$. All fine-structure components of C III λ 1176 are resolved, indicating a low projected rotational velocity.

The carbon abundance is derived from C III λ 1176 and C IV λ 1169. The C III λ 4647-51 recombination lines are also very sensitive to the adopted carbon abundance. The UV lines are well matched, adopting $\mathrm{C/C_\odot} = 0.2$, though they are not very sensitive. A lower abundance, $\mathrm{C/C_\odot} = 0.1$, does not deteriorate the fit much. The TLUSTY OSTAR2002 model does not reproduce C III λ 4650 in emission, due to missing high-excitation levels in the C III model atom that results in underestimating C^{3+} to C^{2+} recombination rate. We calculated a new model with a larger C III model atom, predicting these lines slightly in emission. This issue needs to be reexamined, but we cannot use these lines to derive an abundance with current TLUSTY models. The CMFGEN model includes a better model atom and satisfactorily matches the observed emission with the lower carbon abundance, $\mathrm{C/C_\odot} = 0.1$.

The higher value yields C III lines that are clearly too strong. We have therefore adopted a carbon abundance, $C/C_\odot = 0.1$.

The nitrogen abundance is set by N III λ 1182-84 and N IV λ 1718. A good fit is obtained with an abundance, $N/N_\odot = 0.2$. With this abundance, only very weak N III lines (4097, 4640 Å) are predicted, as observed. The UV lines provide therefore a N/C abundance ratio slightly above solar, contrary to Walborn et al. (2000) suspicion of a low N/C ratio. Actually, nitrogen is not as much enriched as in other stars of our sample, which might have lead them to classify this star as an OC6 star. Conversely, this might suggest that many "normal" O6 V stars might be in fact nitrogen-rich.

A straightforward consequence of the very good agreement between the observed spectrum and the TLUSTY model is that the wind of MPG 113 is weak and the mass loss rate small. Indeed, no P Cygni line profiles are seen in the UV spectrum. The C IV and the N V resonance doublets show a weak signature of the stellar wind (a weak, blueshifted, absorption components), while O V λ 1371 does not reveal any indication of a stellar wind. The comparison of MPG 368 and MPG 113 (Fig. 6 and Fig. 8) is quite striking: while the two stars have a similar effective temperature, the spectral signatures of a wind have almost completely vanished in MPG 113, most likely because of its lower luminosity (about half the luminosity of MPG 368). We shall return to this striking difference in Sect. 6.4 to examine the predictions of the radiatively-driven wind theory.

To derive the wind parameters of MPG 113, we have built a small grid of CMFGEN models, starting with a mass loss rate derived from Vink et al. (2001) formula and decreasing it until we match the observed spectrum. We have adopted a standard wind acceleration, $\beta = 1$, and the parameters derived from the photospheric analysis. We can set an upper limit to the mass loss rate from the C IV doublet, while an homogeneous wind model predicts a strong, unobserved, N V doublet, as well as an (unsaturated) P Cygni profile for O V λ 1371. We examine the role of clumping too, adjusting as before the mass loss rate in order to keep matching the C IV lines. Similarly to the other stars, clumping improves the fit of O V λ 1371, although not as dramatically. The N V lines are also predicted much weaker, but are still predicted significantly too strong. Having set the abundances from photospheric lines, we cannot achieve a good fit of C IV, N V, and O V simultaneously. We have adopted a mass loss rate, $\dot{M} = 3\,10^{-9}\,M_\odot\,yr^{-1}$, for an homogeneous wind (and a mass loss rate three times smaller for a clumped wind) as a best compromise. The predicted C IV blue extended absorption is too weak. The clumped model improves the fit to N V which still remains too strong and it provides a good match to O V. However, the only possible firm conclusion is an upper limit to MPG 113 mass loss rate, $\dot{M} < 10^{-8}\,M_\odot\,yr^{-1}$.

5.5. NGC 346 MPG 487

The hydrogen and helium optical lines as well as the UV C III and C IV lines can be matched with model atmospheres having $T_{\rm eff} = 35\,000$ K and $\log g = 4.0$. The spectrum reveals two main characteristics: *(i)* very narrow and weak metal lines; *(ii)* very weak signatures of a stellar wind similarly to MPG 113. Fitting the metal lines requires to adopt a low microturbulent velocity, $\xi_{\rm t} = 2\,{\rm km\,s^{-1}}$, and a metallicity of one tenth the solar value. A larger microturbulence, e.g. 5 or $10\,{\rm km\,s^{-1}}$, would imply an even lower metallicity. The S V λ1502 is matched satisfactorily by a model spectrum with the lowest microturbulence. Having thus fixed the microturbulent velocity, we have to adopt an oxygen abundance, $O/O_\odot$=0.2, to match the O IV λ1338-43 lines. Once the effective temperature and the microturbulent velocity have been fixed, we can derive the carbon abundance from C III λ1176, 1247 and C IV λ1169, and the nitrogen abundance from N III λ1182-84. The carbon and nitrogen abundances, and thus the N/C abundance ratio, indicates that the surface composition of MPG 487 is quite similar to nebular material in the SMC. Fig. 9 displays the best fits achieved with TLUSTY and CMFGEN model atmospheres.

Despite the very low metallicity derived from the UV spectrum, we are unable to match the visible spectrum. The observed metal lines are very weak (e.g., Si IV λ4088-4116). Some predicted lines (e.g., C III λ4647-50, N III λ4634-40) are even not detected. At face value, the optical spectrum would yield very low upper limits (typically $0.01 \times$ solar) for the abundances of these elements with the adopted stellar parameters (35 000; 4.0).

We suggest that our spectra are contaminated by the presence of one or several additional stars in the slit. As the simplest case, let us imagine that two similar O stars are in the slit, the first one with narrow lines and the second with very broad lines. This would result in a diluted spectrum with weak narrow lines as observed in the UV. The situation in the optical might even be worse due to the fact that the atmospheric seeing could blend the light of more contributors. New observations at very high spatial resolution would therefore be extremely helpful to solve this problem of very weak metal lines in this star. We caution therefore about over-interpreting our results on MPG 487 at this stage.

Like MPG 113, this star reveals no conspicuous P Cygni line profiles in its UV spectrum. The only indication of mass loss is the N V λ1240 resonance doublet. No redshifted emission component is observed, but absorption wings develop bluewards of the rest wavelength of the doublet, extending up to $\approx -1100 \pm 100\,{\rm km\,s^{-1}}$. Because of the low effective temperature that we derived from the photospheric spectrum, N V is not much populated. This detection might suggest that the mass loss rate is not negligible, in order to produce the observed blue absorption wings. However, the photospheric model spectrum calculated from the TLUSTY model reproduce already quite well the C IV λ1549 resonance doublet, suggesting thus that

$\dot{M}$ should remain fairly small. Assuming the carbon and nitrogen abundances determined from the other UV lines (see above), we have calculated a series of CMFGEN models starting with the mass loss rate derived with the Vink et al. (2001) formula ($\dot{M} \approx 10^{-7} M_\odot\,yr^{-1}$). We have decreased the mass loss rate until reaching a satisfactory agreement with the N V and C IV doublets, yielding $\dot{M} \approx 3 \times 10^{-9} M_\odot\,yr^{-1}$. We stress however that this value remains uncertain because N V is a minor ion and that there is no real wind signature in the C IV lines (see Fig. 9). An upper limit, $\dot{M} < 10^{-8} M_\odot\,yr^{-1}$, is nevertheless a robust result. Due to the limited spectral information on the stellar wind, and in particular the absence of O V λ1371 at this low temperature, we cannot establish any meaningful constraint about clumping in the wind. Finally, we point out that the very weak wind lines implies that all stars in the STIS slit must have very weak winds. This might be the case if they all have a sufficiently low luminosity (see §6.3).

5.6. NGC 346 MPG 12

MPG 12 is located at the outskirts of the H II region. Its spectrum is much less contaminated by nebular emission allowing us to make good use of the Balmer and the He I lines in our analysis. MPG 12 was classified as a late O-type star. This is the coolest star of our sample, as evidenced by the weakness of He II lines, of C IV λ1169, and of Fe V lines, and the relative strength of He I lines. We found a good match to the Balmer, He I, and He II lines with (30 000 K; 3.5) and (32 500 K; 3.75) TLUSTY model atmospheres with a metallicity, $Z/Z_\odot = 0.2$. Although the fit seems slightly better for the first model, some degeneracy in stellar parameter space does exist. We have adopted an intermediate model, $T_{\rm eff} = 31\,000$ K and $\log g = 3.6$. This model also reproduces well carbon and iron ionization balances as shown by UV C III-IV and Fe IV-V lines.

At this temperature, we expect neither strong O IV lines nor S V λ1502. We cannot therefore set the microturbulent velocity in the same way than we did with hotter stars. For this purpose, we used mainly iron lines. We found that a model assuming a microturbulent velocity, $\xi_{\rm t} = 5\,{\rm km\,s^{-1}}$, together with a metallicity, $Z/Z_\odot = 0.2$, reproduces well the observed strength of iron lines. We have adopted these values. An alternative solution would be a higher microturbulence ($10\,{\rm km\,s^{-1}}$) together with a lower overall metallicity (one tenth solar), but the adopted model provides a better match to the observations (e.g., the silicon visible lines). The lower metallicity ($Z/Z_\odot = 0.1$) was favored earlier by Lanz et al. (2000). In the meantime, we have improved iron line collisional strengths and showed that the earlier collisional data resulted in lower iron abundances up to a factor 2 (Lanz & Hubeny 2003a).

The carbon abundance was then determined in fitting C III $\lambda\lambda$1176, 1247, 4647-51 and

C IV λ1169. We found that the nebular SMC abundance results in good fits. Similarly, we could use several nitrogen lines, N III λ1183, 4097, 4634-40, and N IV λ1718, to derive the nitrogen abundance. These lines are matched with a solar nitrogen abundance. This results in an N/C abundance ratio 30 times larger than the nebular ratio. This huge surface enrichment was already noticed by Walborn et al. (2000) and Lanz et al. (2000).

MPG 12 shows the weakest spectral wind signatures in our sample. Only slight asymmetries can be observed in the C IV and possibly in the N V resonance lines. We calculated a series of CMFGEN models, proceeding similarly to MPG 113 and MPG 487, starting from the mass loss rate predicted by Vink et al. (2001) and decreasing the mass loss rate until C IV λ1549 is predicted as weak as observed. Homogeneous wind models were assumed and we kept β fixed to unity. This required a quite low mass loss rate for an O star, $\dot{M} = 1 \times 10^{-10}\,\mathrm{M_\odot\,yr^{-1}}$. Lanz et al. (2000) gave a higher mass loss rate ($\dot{M} = 5 \times 10^{-10}\,\mathrm{M_\odot\,yr^{-1}}$) which followed from their adopting a lower carbon abundance.

6. Discussion

Table 3 summarizes the results of our analysis. We conservatively estimate uncertainties to $\pm$5% on $T_{\rm eff}$, $\pm$0.1 dex on $\log g$, and $\pm$2 to $\pm$5 km s^{-1} on $\xi_{\rm t}$ from low to high microturbulent velocities. We do not find any evidence of helium enrichment, and we can thus set a limit on the helium abundances, $y < 0.15$. Typical uncertainties on the other abundances are $\pm$0.1 to $\pm$0.2 dex. The mass loss rates of the three most luminous stars are derived with an accuracy of 10-20 % from the fitting procedure (but this does not include potential systematic errors), while we have mostly obtained limits on the wind properties of the three other stars. We discuss now the implications of our results, comparing them to other observational and theoretical studies.

6.1. Effective Temperatures

The $T_{\rm eff}$ - Spectral Type relation for O stars used most commonly during recent years for studies of young stars and young star-forming regions with massive stars has been established by Vacca et al. (1996). This relation is based on spectroscopic analyses performed in the late 1980's and early 1990's with NLTE H-He model atmospheres. Hubeny et al. (1998) pointed out that the inclusion of metal line blanketing in the NLTE model atmospheres would result in deriving lower effective temperatures. Indeed, several recent studies based on the newest generation of model atmospheres that incorporates the effect of line blanketing point towards

lower $T_{\rm eff}$(Martins et al. 2002; Crowther et al. 2002; Herrero et al. 2002; Bianchi & Garcia 2002).

Martins et al. (2002) have established a new $T_{\rm eff}$ – Spectral Type calibration for Galactic dwarf O stars. Their NLTE line-blanketed model atmospheres, calculated with CMFGEN, predict that line blanketing will result in lowering the effective temperature scale by $\Delta T_{\rm eff}$= 1500 to 4000 K from late to early O-type stars. They have also shown that $\Delta T_{\rm eff}$ is typically only 60% at SMC metallicity (they adopted $Z/Z_{\odot} = 0.125$) compared to changes derived at solar metallicity. This smaller change is expected because the effect of line blanketing is reduced at lower metallicity.

We found effective temperatures that are about 7000 K lower than Vacca et al. (1996) relation for O4V stars, while they are 3000 to 3500 K lower for later O stars. Given the recent redefinition of the earliest spectral types (Walborn et al. 2002), we cannot derive a meaningful conclusion concerning MPG 355. These changes in effective temperature are larger than predicted by Martins et al. (2002), especially for the two stars with early spectral types. We point out however that the early spectral types attributed to MPG 324 and MPG 368 may be an artefact due to the filling of He I lines by nebular emission. If these two stars were classified O6 instead, our results will be more in line with Martins et al. Fig. 11 displays the $T_{\rm eff}$ - Spectral Type relation for Galactic dwarf O stars from Vacca et al. and the improved relation from Martins et al. This figure shows that our temperature estimates are roughly similar or might be somewhat lower than Martin et al.'s, despite the lower metallicity (and presumably a lesser blanketing effect). We have compared our OSTAR2002 model atmospheres calculated at different metallicities, and we confirm that only a part of the difference in $T_{\rm eff}$ can be attributed to the omission of line blanketing in earlier model atmospheres. Thus, we essentially agree with Martins et al. that the inclusion of line blanketing in model atmospheres lowers the deduced effective temperatures, but in addition we argue that the effect is larger than they predicted, likely because of the use of additional temperature indicators like the carbon and iron ionization balance. The magnitude of changes in $T_{\rm eff}$ not as extreme as the changes found by Crowther et al. (2002) for 4 O supergiants in the SMC and in the LMC. Further discussion of the effective temperature scale of O stars at low metallicity will be presented in a separate paper analyzing the full sample of 17 stars observed with HST/STIS in the SMC (Heap et al. 2003a).

6.2. Surface Abundances

Our results on chemical abundances may be summarized in three points:

- These six stars do not reveal any helium enrichment at their surface;
- however, carbon and nitrogren show non-solar abundance ratios;
- the overall metallicity is $Z/Z_{\odot} = 0.2$.

Analyzing a sample of Galactic O stars, Herrero et al. (1992) found that most of them show a helium enrichment at their surface, which was not expected from stellar evolution theory. They termed this problem the "helium discrepancy". The origin of this discrepancy can be attributed to their use of NLTE H-He model atmospheres for the spectroscopic analysis. Stronger He I-II lines are predicted by NLTE line-blanketed model atmospheres. Additionally, Smith & Howarth (1998) argued that a significant microturbulent velocity would strengthen the He lines. High helium abundances would thus be spuriously derived if one assumes that NLTE model atmospheres of O stars should not require any microturbulence to match stellar spectra. Our analysis, based on NLTE line-blanketed model atmospheres and high-resolution spectra, shows that a significant microturbulence is required to match the UV metal lines, and yields solar-like helium abundances. While we cannot exclude small helium enrichments, our results do agree with stellar evolution theory predictions that the surface helium abundance remains mostly unchanged during the main sequence phase of O stars. Even evolutionary models with rotationally-enhanced mixing do not predict significant helium enrichment (Maeder & Meynet 2001). We conclude therefore that the helium discrepancy problem most likely finds its roots in neglecting the role of microturbulence and in neglecting metal line blanketing in the model atmospheres.

In order to interpret the CNO abundance patterns that we have determined in these six stars, we need first to establish a basis for comparison, that is the composition of the original material from which these stars were formed. Venn (1999) summarizes the results of abundances studies in the SMC. While evolved F-K SMC supergiants yield C/N abundance ratios that are similar to the solar neighborhood and young Galactic B stars (N/C$\approx$1/3), SMC nebular studies (Dufour 1984; Garnett et al. 1995) provide a lower abundance ratio, N/C$\approx$1/6 (Venn 1999). There are still uncertainties on the nebular nitrogen abundance in NGC 346. We have adopted a nebular nitrogen abundance, N/N$_{\odot}$=0.03, from Dufour (1984) and Venn (1999), which was supported by recent observations by Peimbert et al. (2000). However, with new photoionization models of NGC 346, Relaño, Peimbert, & Beckman (2002) have argued that the nitrogen abundance might be as high as N/N$_{\odot}$=0.08. They found however that the derived nebular nitrogen abundance is very sensitive to the exact shape of the EUV stellar fluxes. In Table 3, we have listed the derived N/C abundance ratios relative to the nebular ratio, keeping the lower nebular nitrogen abundance. We thus point out that these relative N/C ratio may be reduced by a factor 2 if the Relaño et al. (2002) recent models turn out to predict the correct abundance.

All but one star (MPG 487 which has anomalously weak lines, see §5.5) show a systematic surface enrichment of nitrogen. Moreover, all stars but MPG 355 have a carbon abundance that is consistent with the nebular abundance. Canonical evolutionary models do not predict such a nitrogen surface enrichment during the main sequence phase, but mixing induced by fast rotation may result in such abundance pattern (e.g., Maeder & Meynet 2001). Excluding the anomalous case of MPG 487, the OC6 star remains the least chemically evolved (lowest N/C ratio), corroborating the finding that the OC7.5 III((f)) star AV69 is less evolved than the O7 Iaf+ supergiant AV83 (Hillier et al. 2003). We further examine the evolutionary status of these stars in the following section. Heap et al. (2003b) discuss the surface abundances of the complete stellar sample. Oxygen cannot be derived from this dataset. However, we can argue that our carbon abundances indirectly support the idea that oxygen abundances have to be similar to the nebular value, $O/O_\odot$=0.15-0.19 (Venn 1999; Peimbert et al. 2000). In this analysis, we have adopted $O/O_\odot$=0.2, following the derived metallicity. Additional observations of abundance-sensitive oxygen lines in the near-UV would therefore be a very valuable complement to this study.

Lines of other elements (Si, S, Fe) are well reproduced by adopting scaled-solar abundances. We have derived an overall metallicity, $Z/Z_\odot = 0.2$, in good agreement with previous studies, as summarized by Venn (1999). This value confirms also previous analyses of O stars in the SMC (Haser et al. 1998).

6.3. Evolutionary Status and Age

We compare in Fig. 12 the location of the six studied stars in the HR diagram with predictions of stellar evolution theory. We are using canonical tracks ("normal" mass loss rates, no rotation) from the Geneva group with the appropriate metallicity, $Z/Z_\odot = 0.2$ (Charbonnel et al. 1993). Three stars (MPG 324, 368, and 113) have locations that coincide with an isochrone for $t \approx 3\,10^6$ yr. This agrees well with an early estimate based on a NLTE analysis of optical spectra (Kudritzki et al. 1989), while a younger age of 1 Myr was recently given by Walborn et al. (2000). The later value is based on effective temperatures derived from the spectral type, and the greater age derived from NGC 346 main sequence O stars is now a direct consequence of our lower effective temperature scale.

MPG 355 supported the very young age of NGC 346 derived by Walborn et al. A straightforward interpretation of its location in the HR diagram indeed suggests a very young and massive star ($M \approx 90\,M_\odot, t < 10^6$ yr). Such a massive star would have evolved off the main sequence after 3 Myr. We argue however that so young a star could not show already such an enhancement of its nitrogen surface abundance. Its blue, luminous location might

rather be the consequence of an homogeneous evolution due to rotation near break-up velocity (Maeder 1987b). A $60\,M_\odot$ star with a very fast initial rotation ($v_{\rm rot} \approx 400\,{\rm km\,s^{-1}}$) could have evolved towards MPG 355 location (see Fig. 8 in Meynet & Maeder 2000). From our analysis, we can moreover exclude that MPG 324 and MPG 368 are as hot as $T_{\rm eff} \geq 45\,000\,{\rm K}$. Such a high effective temperature is necessary to assign an age as young as $t \approx 10^6\,{\rm yr}$ to these two stars. A young MPG 355 would therefore not be coeval with them. The older age, $t \approx 3\,10^6\,{\rm yr}$, assuming a homogeneous evolution for MPG 355, seems thus the better alternative.

The location of MPG 487 in the HR diagram indicates that this star is more evolved. Yet, its very weak line spectrum suggests contamination by one or several very close stars (see §5.5). While the effective temperature is determined from line strength ratios, the total luminosity would be overestimated. Therefore, the location of MPG 487 in the HRD is a supportive hint of the multiple nature of the observed object. If we attribute to MPG 487 a luminosity corresponding to the 3 Myr isochrone, the predicted mass loss rate would also be significantly lower and in better agreement with our estimate (see §6.4).

Walborn et al. (2000) already argued that MPG 12 is most likely not a coeval member of the cluster, based on its spatial location outside the nebula, its somewhat discrepant radial velocity, and the derived stellar parameters. Our detailed analysis supports this conclusion, and we derive an age of 8 Myr for this star. MPG 12 is the most evolved star in our sample, showing the highest enhancement in surface nitrogen as may be expected.

6.4. Observed and Predicted Mass Loss Rates

We start by comparing our mass loss rates to Puls et al. (1996) results for Galactic, LMC and SMC stars. Then, we examine how our results compare to theoretical predictions from radiative line-driven wind theory, with an emphasis on the dependence of the mass loss rate on metallicity. First, we will stay in the classical framework of homogeneous, smooth winds. We will then examine the evidence for clumping in the winds of O stars, and discuss the implications of our results for the wind momentum-luminosity relation (WLR). Finally, we shall explore some alternative explanations for the weak winds observed in some stars.

6.4.1. Homogeneous Winds

In the context of the CAK theory of radiatively driven winds (Castor et al. 1975), Abbott (1982) calculated the line force and discussed its dependence with metallicity. He suggested

a dependence of the mass loss rate in the form $\dot{M} \propto Z^m$, with $m \approx 1$. This metallicity dependence was reexamined in later works, resulting in a weaker dependence: Kudritzki et al. (1987) obtained $m \approx 0.5$, while Leitherer et al. (1992) found $m \approx 0.8$. The wind terminal velocities are also found to be significantly smaller at lower metallicities.

The dependence of mass loss on metallicity is most likely the main influence of metallicity on the evolution of massive stars. It is therefore essential to specify better this dependence, in order to provide a firmer basis to model massive stars in very young galaxies. We will first explore this topic empirically, before comparing our results to new theoretical predictions.

We plot in Fig. 13 the mass loss rates derived for Galactic and SMC stars. We use Puls et al. (1996) data, excluding supergiants, and our results. To guide the eye, we have also plotted least-squares fits for Galactic and SMC stars, excluding the three stars with very low mass loss rates. As expected, the mass loss rate is smaller in SMC stars in comparison to Galactic stars. Yet, this difference does not look so well established if we consider only O dwarfs (filled symbols), as the three Galactic dwarf stars are more luminous than their SMC counterparts. The SMC relation is skewed by MPG 355 which is significantly more luminous than other studied SMC stars and was included in the two studies. The least-squares fits suggest that the mass loss rates are 0.2 to 0.6 dex smaller in SMC stars in comparison to Galactic values, with an increasing difference for decreasing luminosities. At lower luminosities, three stars show a precipitous drop of the mass loss rate. Assuming a metallicity, $Z/Z_\odot = 0.2$, the least-squares fit implies a dependence, $\dot{M} \propto Z^m$, with $m = 0.6 \pm 0.3$. While this empirical dependence appears in good agreement with theoretical expectations, we point out that a small m is mostly imposed by MPG 355. Excluding this star, the power law factor is close to unity. A better definition of the metallicity dependence will require additional *homogeneous* analyses of Galactic and SMC main sequence stars.

The dependence of mass loss on stellar metallicity was recently revisited theoretically by Vink et al. (2001). We compare now our results to their predictions. Vink et al. have calculated the mass loss rate for models covering a range in effective temperature, luminosity, and metallicity. The major improvement of their method over previous approaches is to take into account the effect of multiple scattering via a Monte-Carlo technique when calculating the transfer of momentum from the radiation field to matter. They found a relation, $\dot{M} \propto Z^{0.85}$. The relation is even flatter once they factor in the effect of metallicity on the wind terminal velocity, $\dot{M} \propto Z^{0.69}$.

Table 4 lists the stellar parameters required to predict the mass loss rates from Vink et al.'s recipes (their Eq. 24). Since the uncertainty on the stellar masses remain fairly large, we have adopted typical masses for our objects based on the masses listed in Table 3. We have adopted a mass, $M = 65\,M_\odot$, for MPG 355 based on our argument that it might

have undergone homogeneous evolution, and that MPG 355 is rather unlikely to be more massive given NGC 346 age. The escape velocities have been calculated using effective masses derived with Eddington factors, $\Gamma_{\rm e} = 0.434, 0.206, 0.13$, for $\log L = 6.0, 5.5, 5.0$ (Vink et al. 2001). The terminal velocities of Galactic O star winds are related to the escape velocities as $v_\infty \approx 2.6\, v_{\rm esc}$, with an accuracy of 20% (Groenewegen et al. 1989; Lamers et al. 1995; Kudritzki & Puls 2000). The terminal velocities in SMC O stars are smaller by about 20% (Leitherer et al. 1992), and thus $v_\infty/v_{\rm esc} \approx 2.0$. We have measured terminal velocities for the three most luminous stars which agree with these scalings. We could only derive lower limits for the terminal velocities of the three other stars, and we have therefore adopted terminal velocities that are twice the escape velocities. We apply Vink et al.'s Eq. 24 using a metallicity, $Z/Z_\odot = 0.2$.

The predicted and measured mass loss rates for MPG 355, MPG 324 and MPG 368, are in reasonable agreement. This conclusion holds however only if we compare mass loss rates derived from homogeneous wind models (as assumed by Vink et al.). While the agreement is excellent for MPG 355, our mass loss rates measured for the two other stars are about half the predicted ones. If we were to adopt a larger mass, $M = 90\, M_\odot$, for MPG 355, this conclusion would not be changed. On the other hand, we find dramatic differences for the three other stars: their mass loss rates are 1 to 2 orders of magnitude smaller than predicted. This discrepancy may be smaller for MPG 487 if we assume a lower luminosity to correct from its probable multiple nature. Assuming $\log L \approx 4.6$ and $M \approx 20\, M_\odot$, corresponding to a 3 Myr old star with $T_{\rm eff}$=35 000 K, the predicted mass loss rate is decreased to $\dot{M}$=$10^{-8}\,{\rm M}_\odot\,{\rm yr}^{-1}$. This is still a factor 3.5 higher than the observed value. We compare measured and predicted mass loss rates in Fig. 14, including also results from Puls et al. (1996) and Hillier et al. (2003). While Vink et al.'s relation appears to provide a good agreement with mass loss rates measured for evolved stars, it clearly overestimate the mass loss rate of main-sequence SMC O stars. As an illustration, we display in Fig. 15 the predicted profiles for MPG 113 calculated assuming Vink et al. mass loss rate. The mass loss rate is corrected by a factor, $(f_\infty)^{0.5} = 0.1^{0.5}$, for the clumped model. Clearly, we cannot match the observed line profiles with this mass loss rate, or we would need very low, unrealistic CNO abundances. Hillier et al. (2003) found mass loss rates that 2 to 3 times larger than the theoretical values. They argued however that AV 83 mass loss is most likely enhanced due to fast rotation. Fig. 16 displays the ratio of predicted to measured mass loss rates as a function of the stellar luminosity. Most clearly, the theoretical predictions do not account for thin winds and low luminosity main sequence stars ($L < 3\,10^5\, L_\odot$). Three brighter stars in Puls et al. sample ($L \approx 5\,10^5\, L_\odot$) also show much weaker winds than expected. Furthermore, we point out that Vink et al.'s predictions also overestimate Puls et al. measurements for giant/supergiants in the LMC. These results may therefore suggest a steeper dependence than currently predicted by the

radiatively line-driven theory ($\dot{M} \propto Z^{0.5-0.7}$). Vink et al.'s method consists in estimating the mass loss that can be driven by the star to an observed v_∞. Their method assumes but does not show that such a mass loss can be driven through the sonic point. This might be the underlying reason why they systematically overestimate the mass loss rates.

Our understanding of the mass loss dependence with metallicity remains therefore sketchy, and cast some doubts on our ability to extrapolate the results obtained on Magellanic Clouds stars to the very low metallicity environment of young galaxies. Detailed studies of larger sample of O stars at low metallicity would therefore be very valuable. We also need to establish a larger reference set of Galactic stars using similar high-quality spectroscopic data and the same modeling techniques.

6.4.2. Clumped Winds

Clumping in the wind introduces an additional complication in determining the actual mass loss rates. In order to reproduce adequately the weak incoherent electron scattering wings of He II lines, Hillier (1991) already suggested over 10 years ago that the dense winds of Wolf-Rayet stars might be clumped. Inclusion of clumping resulted in revising down by a factor 2 the mass loss rates of Wolf-Rayet stars (Hamann & Koesterke 1998). While Puls et al. (1996) have considered the effect on Hα of clumping in O star winds, first evidences of clumping in the wind of O supergiants were submitted only recently. Eversberg et al. (1998) argued that stochastic variable substructures in He IIλ4686 reveal the presence of outmoving clumps in the wind of the O4 supergiant ζ Puppis. Crowther et al. (2002) and Hillier et al. (2003) provided further arguments from spectroscopic analyses that O supergiant winds are clumped, based namely on the P V resonance lines and on the absence of blue asymmetry in strong photospheric lines in AV 83.

The inability of standard, smooth O star wind models to reproduce O V λ1371 is a long-standing problem. We point out that the absorption and the emission components are always systematically predicted too strong, by wind models assuming a β-velocity law as well as by models solving for the hydrodynamical structure. This failure is therefore not a consequence of adopting an empirical velocity/density law. Several solutions have been envisaged, including lower effective temperatures (de Koter et al. 1998) or lower oxygen abundances (e.g. Haser et al. 1998). While these two solutions decrease the O V line strength, there are no other supporting evidences for them; moreover, they are not improving on the qualitative disagreement between predicted and observed line shapes. In this paper, we have achieved for the first time a good match of O V λ1371 line, assuming the simple clumping recipes incorporated in CMFGEN. We used a volume clumping factor, $f_\infty \approx 0.1$,

consistent with previous studies of clumped winds, for the three stars with $T_{\rm eff} \approx 40\,000$ K. A smaller clumping factor, $f_\infty = 0.01$, yields a better fit for the hottest star, MPG 355, but results in an unrealistic large line driving force. To drive MPG 355 observed wind, our calculations of line driving forces support clumping, but with a filling factor somewhat larger than 0.1. At the current point, we think that this shows that clumped models predict, correctly or by coincidence, the O IV/O V density around the sonic point and in the wind, and thus match O V λ1371. Lacking reliable estimates of the oxygen abundance remains a major uncertainty. We feel therefore that it is still somewhat premature to claim that O star winds are clumped. However, since this conclusion has potentially foremost consequences for stellar evolution in reducing the mass loss rates of massive stars, we believe that clumping needs to be further investigated, building a consistent model of O V, P V, and strong photospheric lines while deriving oxygen abundances independently.

6.4.3. Wind Asymmetries

We have pointed out that our wind models predict too strong a N V λ1240 emission component in all cases, even though we have not accounted for the increased ionization due to shocks in the wind. We notice that Haser et al. (1998) also predict too strong N V emission in their analysis of two SMC stars, MPG 355 and AV 243, although their models fit the observed profile of two LMC stars well. Effective temperatures, nitrogen abundances, and mass loss rates, have been derived by matching other lines. Fitting the observed N V λ1240 line profiles would require incompatible changes in these parameters. Clumping helps a little, but does not solve the inconsistency fully. Adopting slightly lower nitrogen abundances might also lessen this discrepancy.

On the other hand, we recall that our sample has been selected with a bias towards stars with sharp-lined spectra. Given the fast intrinsic rotation of O stars, we are viewing our sample stars preferentially pole-on. Owocki et al. (1998) have argued that gravity darkening effects can lead to a reduced mass loss, and thus lower density, in the equatorial region of the wind, contrary to earlier studies of a Wind Compressed Disk model (Bjorkman & Cassinelli 1993). The lower equatorial density would thus result in weaker emission components in stars seen pole-on. Further analyses of unbiased stellar samples are necessary in order to support our suspicion.

6.4.4. Wind Momentum-Luminosity Relation

We display the modified Wind momentum-Luminosity relation (WLR) in Fig. 17, where we compare the WLR for Galactic and SMC stars. The wind momentum of the three brightest stars of our sample (MPG 355, 324, and 368) agrees well with values derived for other SMC stars. Least-squares fits through Galactic supergiants and SMC stars ($\log L > 5.4$) have a very similar slope, $1/\alpha' \approx 1.9$, and are comparable to a value derived by Puls et al. (1996). The offset between the two relations can be interpreted as an effect of metallicity and implies, $\dot{M}v_\infty \propto Z^m$, with $m = 0.87$. Allowing for a metallicity dependence of the wind terminal velocities, $v_\infty \propto Z^{0.13}$ (Leitherer et al. 1992), we obtain a dependence of the mass loss rate, $\dot{M} \propto Z^{0.74}$, which agrees well with theoretical expectations. However, we should point out that the Galactic relation is established for supergiants, while the SMC relation is based mostly on giants and dwarfs. The few Galactic dwarfs fell clearly below the supergiant relation and, therefore, the difference in wind momentum between Galactic and SMC dwarfs is significantly reduced (by a factor 2 at least). On the other hand, evolved SMC stars like AV 83 and AV 69 have a wind momentum that is quite similar to these of Galactic supergiants.

A second interesting feature of the WLR is the steep turn at low luminosity ($\log L < 5.5$). This behavior was already noticed by Puls et al. (1996) for a few Galactic and SMC stars, though the drop may start at higher luminosity at low metallicity. The three low luminosity stars in our sample confirm this steeper trend, as well as recent results in the star forming region N81 in the SMC where low luminosity OVz stars reveal very weak wind signatures (Martins et al. 2003). This break in the WLR appears to be primarily related to the stellar luminosity, not to the effective temperature because low wind momentum spans a range in $T_{\rm eff}$, from 45 000 to 30 000 K. This break is therefore not related to bistability jumps that are predicted by Vink et al. (and references therein). They predict a jump around 35 000 K with an increase of the mass loss rate toward lower $T_{\rm eff}$, albeit at metallicities much lower (1/30 solar) than those considered here.

We have also plotted WLR data for three early B supergiants with $T_{\rm eff} \approx 28\,000$ K (Kudritzki et al. 1999; Herrero et al. 2002). The O supergiant WLR can be extended to the lower luminosity, $\log L < 5$, for two of these B supergiants. This shows therefore a striking difference in the wind properties of early B supergiants and low luminosity O stars. A stronger wind might be driven by the B supergiants due to their lower surface gravity, $\log g = 3.0 - 3.2$, compared to O stars ($\log g = 4.0$). Cooler B supergiants ($T_{\rm eff} < 25\,000$ K) have a lower wind momentum because the wind is then driven by lines of another set of ions (Kudritzki et al. 1999). We are currently obtaining STIS spectra of B supergiants in the SMC which will allow us to further study the WLR.

6.4.5. Wind Decoupling

Other mechanisms might account for the weak winds that we observe. First, Owocki & Puls (1999) suggested that for stars with optically thin continuum near the sonic point, i.e stars with low luminosities and/or low metallicity, the velocity field in the sonic region is such that the line accelerations are significantly lower than previously considered in the Sobolev formalism. As a consequence, the wind properties are significantly modified, and mass-loss rates are smaller. Furthermore, investigating the instability caused by heavy (minor) ions runaway in low-density line-driven winds, Owocki & Puls (2002) have derived a scaling relation for the stellar winds parameters at which a decoupling between minor ions and the bulk of the hydrogen-helium wind can occur. Applying this relation to our sample, we found that decoupling may indeed occur over most parts of the winds of MPG 12, 487, and 113.

6.4.6. Hydrodynamics

Because the CMFGEN models are fully line-blanketed, it is possible to check the consistency between the derived wind parameters ($\dot{M}$, v_∞, and β) and the computed line force. For simplicity, we consider two stars: MPG 113 and MPG 355. To improve the accuracy of the line force calculations, the models discussed here include Ar, S, Cl, and Ni, in addition to the elements listed in Table 2.

We have derived a very low mass loss rate ($\dot{M} < 10^{-8}\,\mathrm{M_\odot\,yr^{-1}}$) for MPG 113, with inhomogeneous wind models having a mass loss rate a factor up to 10 lower. With the derived mass-loss rate(s) the radiative acceleration is much larger than that required to drive the wind. This is verified even for a model in which we adopt, $\dot{M} = 10^{-8}\,\mathrm{M_\odot\,yr^{-1}}$, $f_\infty = 0.1$, and $v_\infty = 2200\,\mathrm{km\,s^{-1}}$. In this model, the radiative acceleration is a factor of two too large in the outer region, and exceeds that required to drive the wind except for two depths near the sonic point. The discrepancy near the sonic point is not unusual – the radiation force is very sensitive to the velocity law and to the adopted microturbulent velocity in this region (see a discussion in Hillier et al. 2003).

How can we resolve this wind-momentum discrepancy? Three solutions readily manifest themselves:

1. There is a problem in the computed CMFGEN ionization which affects the derived mass loss rates. This discrepancy could arise from several different sources including inaccurate atomic data, the influence of X-rays, and CMFGEN's approximate treatment of clumping. We note (Sect. 5.1) that many tests were performed to verify CMFGEN, and

no major changes in the derived mass loss rate was obtained. Moreover, we note that the problem with fitting O Vλ1371 has been a problem in all other wind calculations (e.g., Haser et al. (1998)).

2. Wind decoupling (Sect. 6.4.5).

3. The adopted v_∞ is too low. As noted, v_∞ cannot be derived from the observations. If v_∞ was much higher than 2000 km s^{-1}, the discrepancy might be lowered.

For MPG 355, v_∞ is well determined, and the principal uncertainty in checking the hydrodynamics is the volume filling factor. For $f_\infty = 1.0$, the radiation force is too low to drive the adopted mass loss rate throughout the entire wind. The line radiation force needs to be increased by 20 to 90% (depth-dependent, and excluding the sonic region) to drive the wind.

For $f_\infty = 0.1$, there is a better agreement with the hydrodynamics, in general. In the outer region, the line force is too small by 20%, while at $v_\infty/2$ it is 30% too large. Given the uncertainties in the adopted velocity law and abundances, these differences are within expected errors, and could probably be remedied with slightly different but similar models. The line force is still much too small at the sonic point, but this is not surprising given the large adopted turbulent velocity, ξ_t =25 km s^{-1}.

For $f_\infty = 0.01$, the line force is larger than that required to drive the wind at all locations with $v(r)$ >70 km s^{-1}. Throughout the wind, the line force is too large by at least a factor of two. We have not included Ar, S, Cl, and Ni, in this model; hence, a full model will show an even larger discrepancy. It is thus difficult to see how such a model could be adjusted to give consistency between both the observed spectrum and the wind hydrodynamics.

7. Conclusions

We have analyzed the UV and optical spectrum of six young, massive O stars in NGC 346, the largest H II region in the SMC. We summarize here our main findings:

- Similarly to several recent studies, we have derived lower effective temperatures than values obtained from a standard relation with the spectral type. This results in lower stellar luminosities and lower ionization fluxes from lower bolometric corrections. Taking MPG 324 as an example, the effective temperature is lowered from 48 670 K (from O4V spectral type) to 41 500 K, decreasing the luminosity by a factor 1.6 and the number of Lyman continuum photons by a factor 2.

- Some microturbulence is still required to match the UV metal lines. Our analysis hints at a decrease of the microturbulent velocity from early to late O stars, from a value close to the sonic velocity down to a low value, 2 to $5\,\mathrm{km\,s^{-1}}$. Having set the microturbulence independently from UV metal lines, we are able to match the helium lines in the optical spectrum without requiring a surface enrichment.

- Most stars have a carbon abundance similar to the SMC nebular abundance, but their surface is markedly enriched in nitrogen already during the MS phase. Either, most are fast rotators viewed pole-on or mixing efficiency is underestimated by current evolutionary models.

- Young SMC O stars have an overall metallicity, $Z/Z_\odot = 0.2$, that is consistent with evolved F-K supergiants.

- The dependence of the mass loss rate with metallicity is consistent with a relation, $\dot{M} \propto Z^m$, with $0.5 > m > 1.0$. A better characterization of m requires larger stellar samples and detailed analysis of high-quality spectra. We have obtained very low mass loss rates for three stars, which cannot be explain in the framework of radiative line-driven wind, but may indicate decoupling between hydrogen, helium, and metals, in the wind. Vink et al. (2001) predict significantly too high mass loss rates for SMC and for LMC stars. Use or extrapolation of their relations at sub-solar metallicities should be taken with caution.

- Homogeneous, smooth winds predict too strong N V λ1240 and O V λ1371 lines, suggesting that the winds of O dwarfs may be clumped or asymmetric, similarly to winds of O supergiants and WR stars.

- Finally, we have achieved a very good consistency between TLUSTY and CMFGEN models. This agreement demonstrates that we can use NLTE photospheric, static model atmospheres to derive stellar parameters and abundances, even for the hottest O dwarfs with moderate winds ($\dot{M} \approx$ few $10^{-6}\,\mathrm{M_\odot\,yr^{-1}}$, assuming $\beta = 1$).

This work was supported by a NASA-NRC Research Associateship at GSFC (JCB), and by grants (GO 7437, AR 7985) from the Space Telescope Science Institute, which is operated by the Association of Universities for Research in Astronomy, Inc., under NASA contract NAS5-26555. We thank the referee, Paul Crowther, for helpful comments. TL enjoyed the warm mediterranean hospitality at Laboratoire d'Astrophysique de Marseille during the completion of this paper.

REFERENCES

Abbott, D. C. 1982, ApJ, 259, 282

Bianchi, L., & Garcia, M. 2002, ApJ, 581, 610

Bjorkman, J. E., & Cassinelli, J. P. 1993, ApJ, 409, 429

Castor, J. I., Abbott, D. C., & Klein, R. I. 1975, ApJ, 195, 157

Charbonnel, C., Meynet, G., Maeder, A., Schaller, G., & Schaerer, D. 1993, A&AS, 101, 415

Chlebowski, T., & Garmany, C. D. 1991, ApJ, 368, 241

Conti, P. S., Leitherer, C., & Vacca, W. D. 1996, ApJ, 461, L87

Crowther, P. A., Hillier, D. J., Evans, C. J., Fullerton, A. W., De Marco, O., & Willis, A. J. 2002, ApJ, 579, 774

de Koter, A., Heap, S. R., & Hubeny, I. 1998, ApJ, 509, 879

Dufour, R. J. 1984, in Structure and evolution of the Magellanic Clouds, Proc. IAU Symp. 108, S. van den Bergh & K. S. de Boer (eds), (Dordrecht: Reidel), 353

Eversberg, T., Lépine, S., & Moffat, A. F. J. 1998, ApJ, 494, 799

Garnett, D. R., Skillman, E. D., Dufour, R. J., Peimbert, M., Torres-Peimbert, S., Terlevich, E., & Shields, G. A. 1995, ApJ, 443, 64

Grevesse, N., & Sauval, A. 1998, Space Sci. Rev., 85, 161

Groenewegen, M. A. T., Lamers, H. J. G. L. M., & Pauldrach, A. W. A. 1989, A&A, 221,78

Hamann, W.-R., & Koesterke, L. 1998, A&A, 335, 1003

Haser, S. M., Pauldrach, A. W. A., Lennon, D. J., Kudritzki, R. P., Lennon, M., Puls, J., & Voels, S. A. 1998, A&A, 330, 285

Hauschildt, P. H., Baron, E., & Allard, F. 1997, ApJ, 483, 390

Heap, S. R., & Lanz, T. 2003, to appear in Stellar Rotation, Proc. IAU Symp. 215, Eds. A. Maeder & P. Eenens, ASP Conf. Ser.

Heap, S. R., Lanz, T., et al. 2003a, in preparation

Heap, S. R., Lanz, T., et al. 2003b, in preparation

Herrero, A., Kudritzki, R. P., Vilchez, J. M., Kunze, D., Butler, K., & Haser, S. 1992, A&A, 261, 209

Herrero, A., Puls, J., & Najarro, F. 2002, A&A, 396, 949

Hillier, D. J. 1991, A&A, 247, 455

Hillier, D. J. 1997, in Wolf-Rayet Stars in the Framework of Stellar Evolution, Proc. 33rd Liège Intern. Astr. Coll., J. M. Vreux et al. (eds), 509

Hillier, J. D. 2003, in Stellar Atmospheres Modeling, Eds. I. Hubeny et al., ASP Conf. Ser., 288, 199

Hillier, D. J., & Miller, D. L. 1998, ApJ, 496, 407

Hillier, D. J., Lanz, T., Heap, S. R., Hubeny, I., Smith, L. J., Evans, C. J., Lennon, D. J., & Bouret, J.-C. 2003, ApJ, 588, 1039

Hubeny, I., & Lanz, T. 1995, ApJ, 439, 875

Hubeny, I., Heap, S. R., & Lanz, T. 1998, in Boulder-Munich II: Properties of Hot, Luminous Stars, I. Howarth (ed), ASP Conf. Ser., 131, 108

Hubeny, I., Mihalas, D., & Werner, K. (eds) 2003, Stellar Atmospheres Modeling, ASP Conf. Series, 288 (San Francisco: ASP)

Koesterke, L., Hamann, W.-R., & Graefener, G. 2002, A&A, 384, 562

Kudritzki, R. P.1992, A&A, 266, 395

Kudritzki, R. P., & Puls, J. 2000, ARA&A, 38, 613

Kudritzki, R. P., Pauldrach, A., & Puls, J. 1987, A&A, 173, 293

Kudritzki, R. P., Cabanne, M. L., Husfeld, D., Niemela, V. S., Groth, H. G., Puls, J., & Herrero, A. 1989, A&A, 226, 235

Kudritzki, R. P., Puls, J., Lennon, D. J., Venn, K. A., Reetz, J., Najarro, F. , McCarthy, J. K., & Herrero, A. 1999, A&A, 350, 970

Lamers, H. J. G. L. M., Snow, T. P., & Lindholm, D. M. 1995, ApJ, 455, 269

Lanz, T., & Hubeny, I. 2003a, in Stellar Atmospheres Modeling, Eds. I. Hubeny et al., ASP Conf. Ser., 288, 117

Lanz, T., & Hubeny, I. 2003b, ApJS, 146, 417

Lanz, T., Bouret, J.-C., Heap, S. R., et al. 2000, AAS, 197, 78.11

Leitherer, C., Robert, C., & Drissen, L. 1992, ApJ, 401, 596

Lindler, D. J 1999, http://hires.gsfc.nasa.gov/stis/docs/calstis/calstis.ps

Maeder, A. 1987a, A&A, 173, 247

Maeder, A. 1987b, A&A, 178, 159

Maeder, A., & Meynet, G. 2000, ARA&A, 38, 143

Maeder, A., & Meynet, G. 2001, A&A, 373, 555

Martins, F., Schaerer, D., & Hillier, D. J. 2002, A&A, 382, 999

Martins, F., Schaerer, D., & Heydari-Malayeri, M. 2003, in A massive star odyssey: from main-sequence to supernova, Proc. IAU Symp. 212, K. A. van der Hucht et al. (eds), ASP Conf. Series, in press

Massey, P., Parker, J. W., & Garmany, C. D. 1989, AJ, 98, 1035

Meynet, G., & Maeder, A. 2000, A&A, 361, 101

Nahar, S. N. 1999, ApJS, 120, 131

Niemela, V. S., Marraco, H. G., & Cabanne, M. L. 1986, PASP, 98, 1133

Owocki, S. P., & Puls, J. 1999, ApJ, 510, 355

Owocki, S. P., & Puls, J. 2002, ApJ, 568, 965

Owocki, S. P., Cranmer, S. R., & Gayley, K. G. 1998, Ap&SS, 260, 149

Pauldrach, A. W. A., Hoffmann, T. L., & Lennon, M. 2001, A&A, 375, 161

Peimbert, M., Peimbert, A., & Ruiz, M. T. 2000, ApJ, 541, 688

Petrenz, P., & Puls, J. 1996, A&A, 312, 195

Prinja, R. K., & Crowther, P. A. 1998, MNRAS, 300, 828

Puls, J., Kudritzki, R. P., Herrero, A., Pauldrach, A. W. A., Haser, S. M., Lennon, D. J., Gabler, R., Voels, S. A., Vilchez, J. M., Wachter, S., & Feldmeir, A. 1996, A&A, 305, 171

Relaño, M., Peimbert, M., & Beckman, J. 2002, ApJ, 564, 704

Schaerer, D., & Schmutz, W. 1994, A&A, 288, 231

Sellmaier, F., Puls, J., Kudritzki, R. P., Gabler, A., Gabler, R., & Voels, S. A. 1993, A&A, 273, 533

Smith-Neubig, M., & Bruhweiler, F. 1997, AAS, 191, 76.09

Smith, K. C., & Howarth, I. D. 1998, MNRAS, 299, 1146

Steidel, C. C., Giavalisco, M., Pettini, M., Dickinson, M., & Adelberger, K. L. 1996, ApJ, 462, L17

Taresch, G., Kudritzki, R. P., Hurwitz, M., Bowyer, S., Pauldrach, A. W. A., Puls, J., Butler, K., Lennon, D. J., & Haser, S. M. 1997, A&A, 321, 531

Vacca, W. D., Garmany, C. D., & Shull, J. M. 1996, ApJ, 460, 914

Venn, K. A. 1999, ApJ, 518, 405

Vink, J. S., de Koter, A., & Lamers, H. J. G. L. M. 2000, A&A, 362, 295

Vink, J. S., de Koter, A., & Lamers, H. J. G. L. M. 2001, A&A, 369, 574

Walborn, N. R. 1978, ApJ, 224, L133

Walborn, N. R., & Blades, J. C. 1986, ApJ, 304, L17

Walborn, N. R., Lennon, D. J., Haser, S. M., Kudritzki, R. P., & Voels, S. A. 1995, PASP 107, 104

Walborn, N. R., Lennon, D. J., Heap, S. R., Lindler, D. J., Smith, L. J., Evans, C. J., & Parker, J. W. 2000, PASP, 112, 1243

Walborn, N. R., Howarth, I. D., Lennon, D. J., Massey, P., Oey, M. S., Moffat, A. F. J., Skalkowski, G., Morrell, N. I., Drissen, L., & Parker, J. W. 2002, PASP, 123, 2754

This preprint was prepared with the AAS LaTeX macros v5.0.

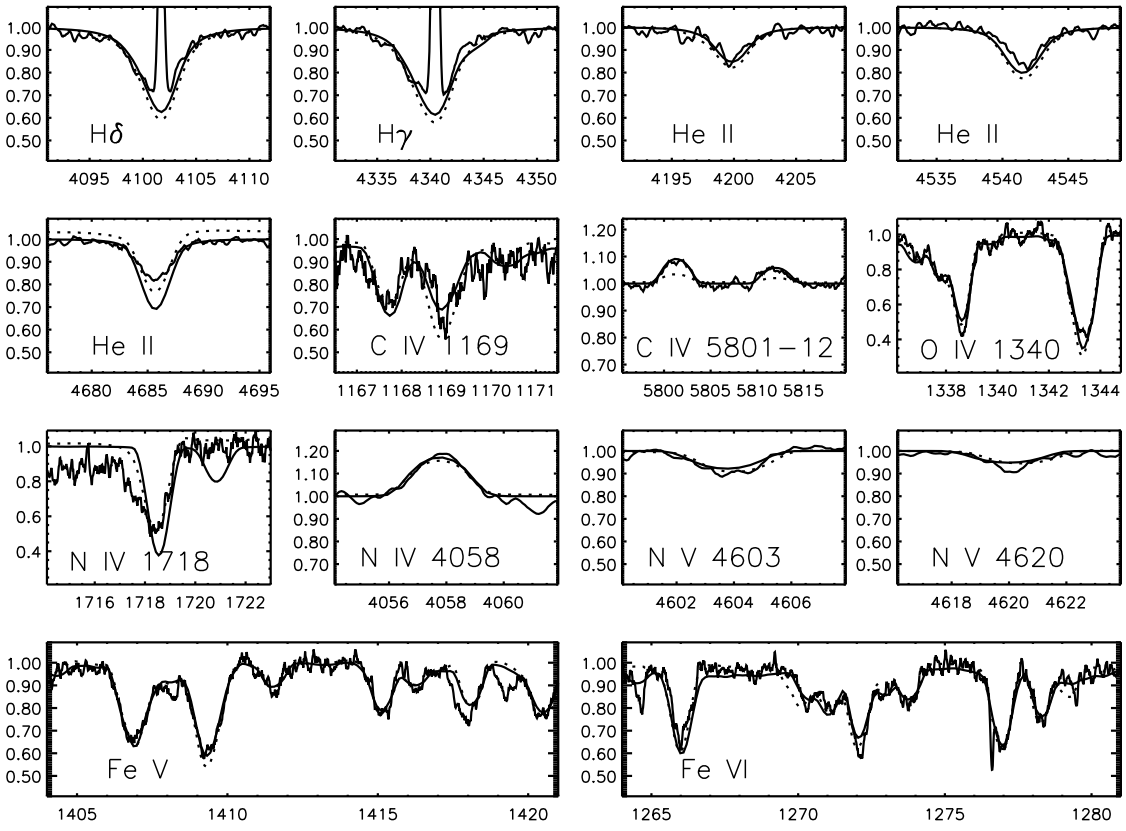

Fig. 1.— Best fits to MPG 355 "photospheric" lines used to derive the stellar parameters, $T_{\rm eff}$=52500 K, $\log g = 4.0$, and surface chemical composition, $Z/Z_\odot = 0.2$ (full line: TLUSTY, dotted line: CMFGEN).

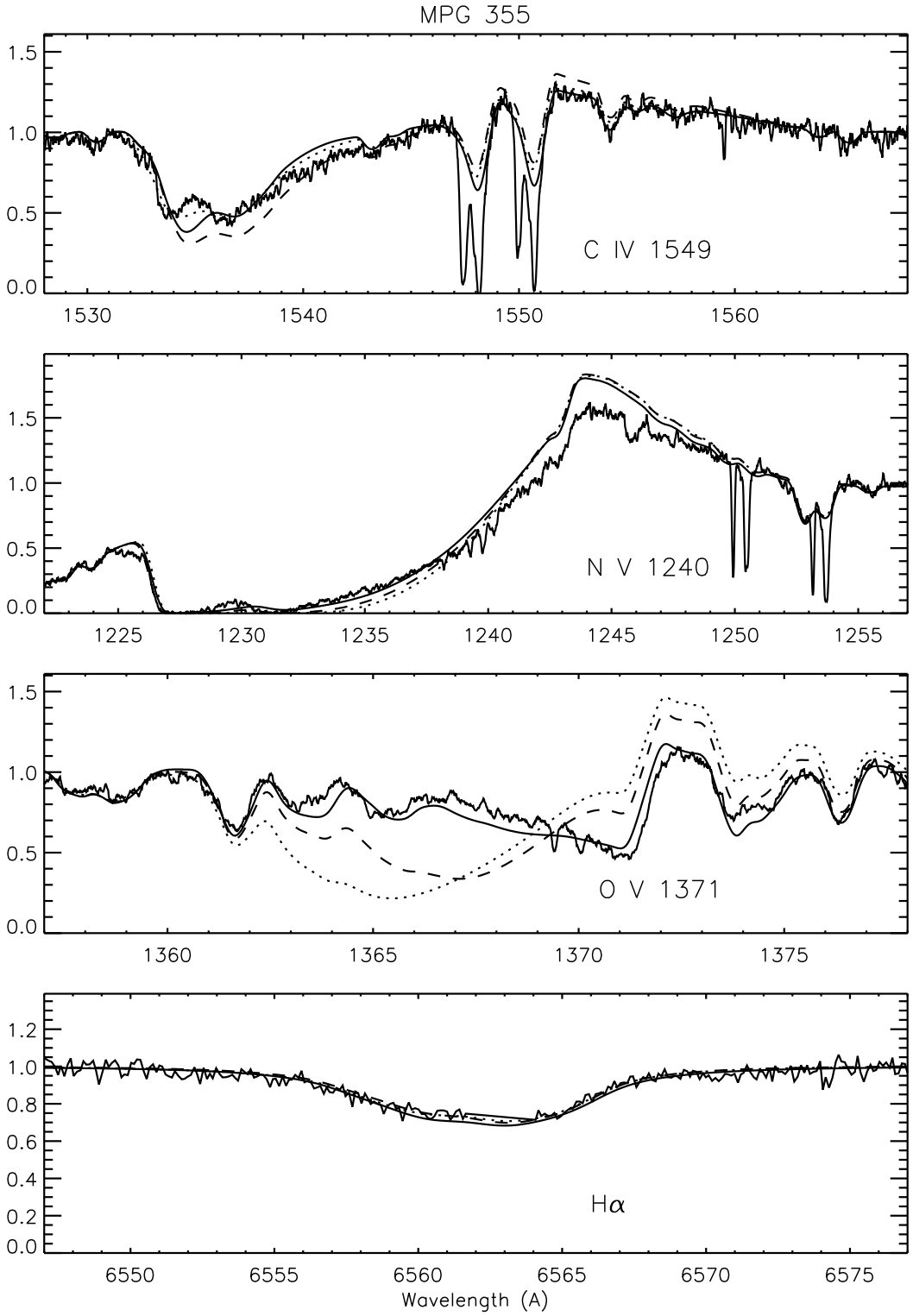

Fig. 2.— Influence of clumping on MPG 355 wind lines. A comparison of three models with different clump volume filling factors: no clumps, $f_\infty = 1.0$ (dotted); $f_\infty = 0.1$ (dashed); and best fit, $f_\infty = 0.01$ (full line). The mass loss rates have been adjusted to match the C IV λ1549 lines, and are $\dot{M} = 2.5 \times 10^{-6}$, 7.9×10^{-7}, and $1.8 \times 10^{-7}\,M_\odot\,yr^{-1}$, respectively. The blue side of N V λ1240 is affected by interstellar Ly α absorption. For display purposes, the core of Hα was cut off to remove nebular contributions.

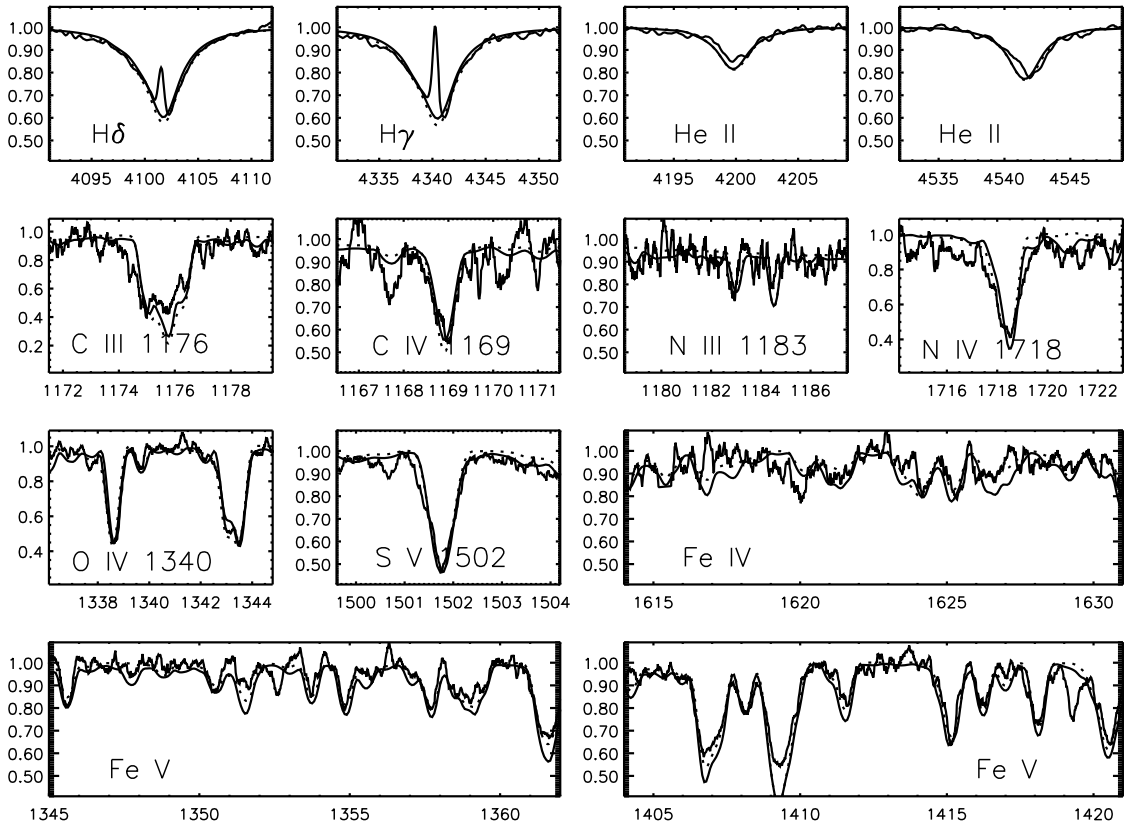

Fig. 3.— Best fits to MPG 324 photospheric lines used to derive the stellar parameters, $T_{\rm eff}$=41500 K, $\log g = 4.0$, and surface chemical composition, $Z/Z_{\odot} = 0.2$ (full line: TLUSTY, dotted line: CMFGEN).

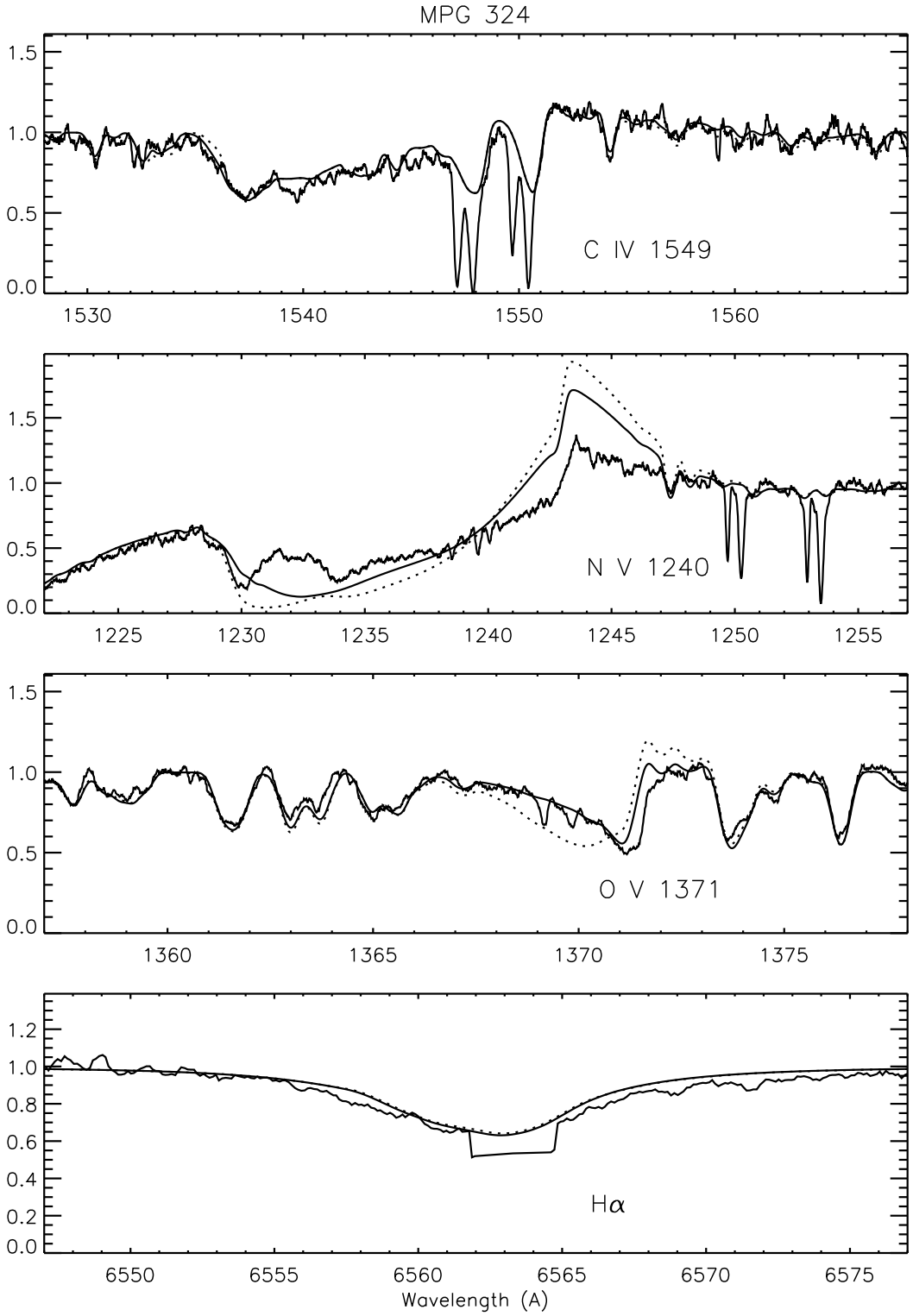

Fig. 4.— Influence of clumping on MPG 324 wind lines. A comparison of two models with different clump volume filling factors: no clumps, $f_\infty = 1.0$ (dotted); and best fit, $f_\infty = 0.1$ (full line). The mass loss rates have been adjusted to match the C IV λ1549 lines, and are $\dot{M} = 2.7 \times 10^{-7}$, and $1.0 \times 10^{-7}\,M_\odot\,yr^{-1}$, respectively. The blue side of N V λ1240 is affected by interstellar Ly α absorption. For display purposes, the core of Hα was cut off to remove nebular contributions.

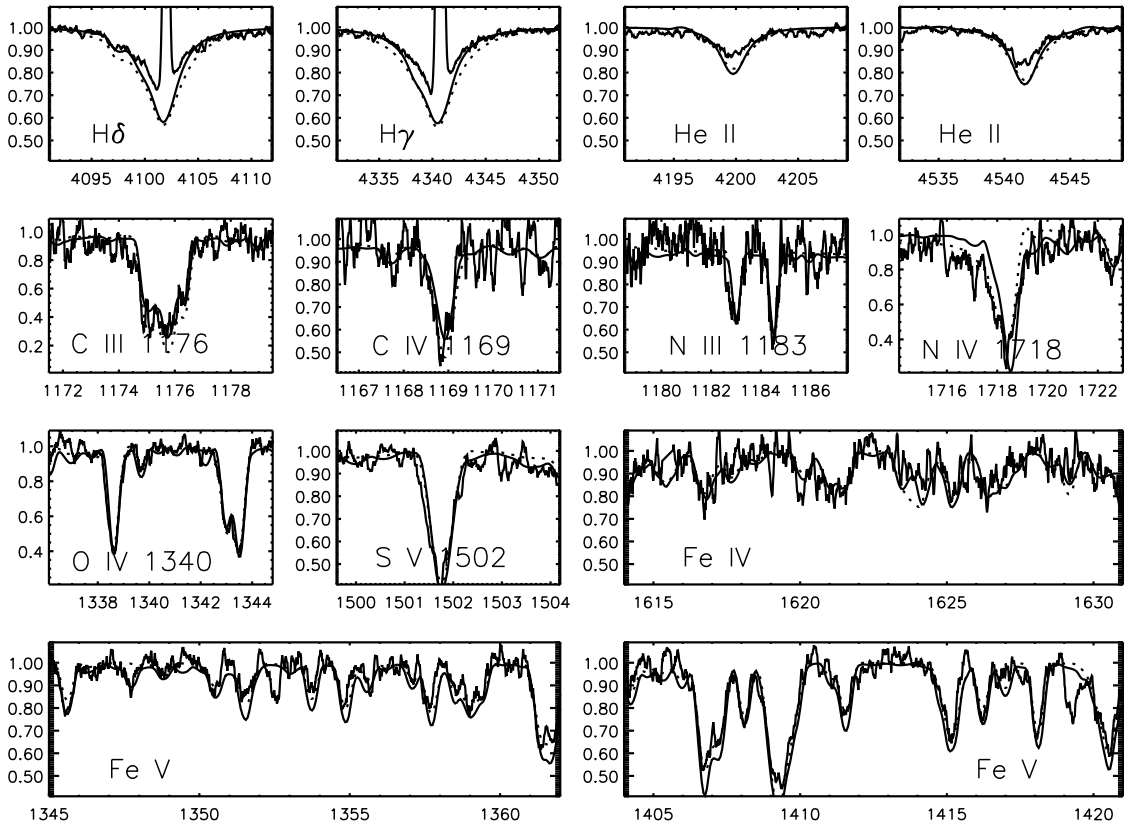

Fig. 5.— Best fits to MPG 368 photospheric lines used to derive the stellar parameters, $T_{\rm eff}$=40000 K, $\log g = 3.75$, and surface chemical composition, $Z/Z_\odot = 0.2$ (full line: TLUSTY, dotted line: CMFGEN).

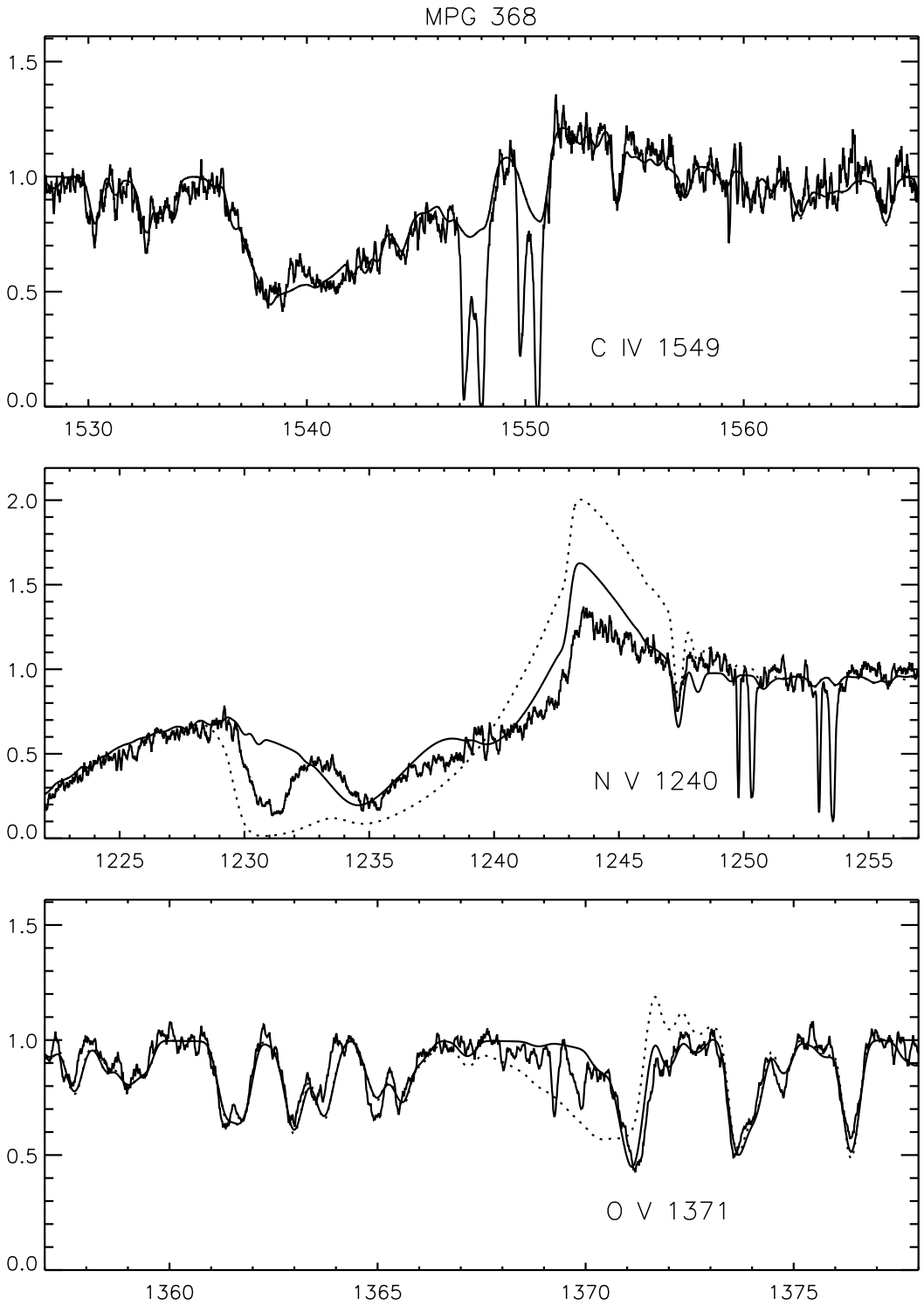

Fig. 6.— Influence of clumping on MPG 368 wind lines. A comparison of two models with different clump volume filling factors: no clumps, $f_\infty = 1.0$ (dotted); and best fit, $f_\infty = 0.05$ (full line). The mass loss rates have been adjusted to match the C IV λ 1549 lines, and are $\dot{M} = 1.5 \times 10^{-7}$, and $5.7 \times 10^{-8}\,\mathrm{M}_\odot\,\mathrm{yr}^{-1}$, respectively. The blue side of N V λ1240 is affected by interstellar Ly α absorption.

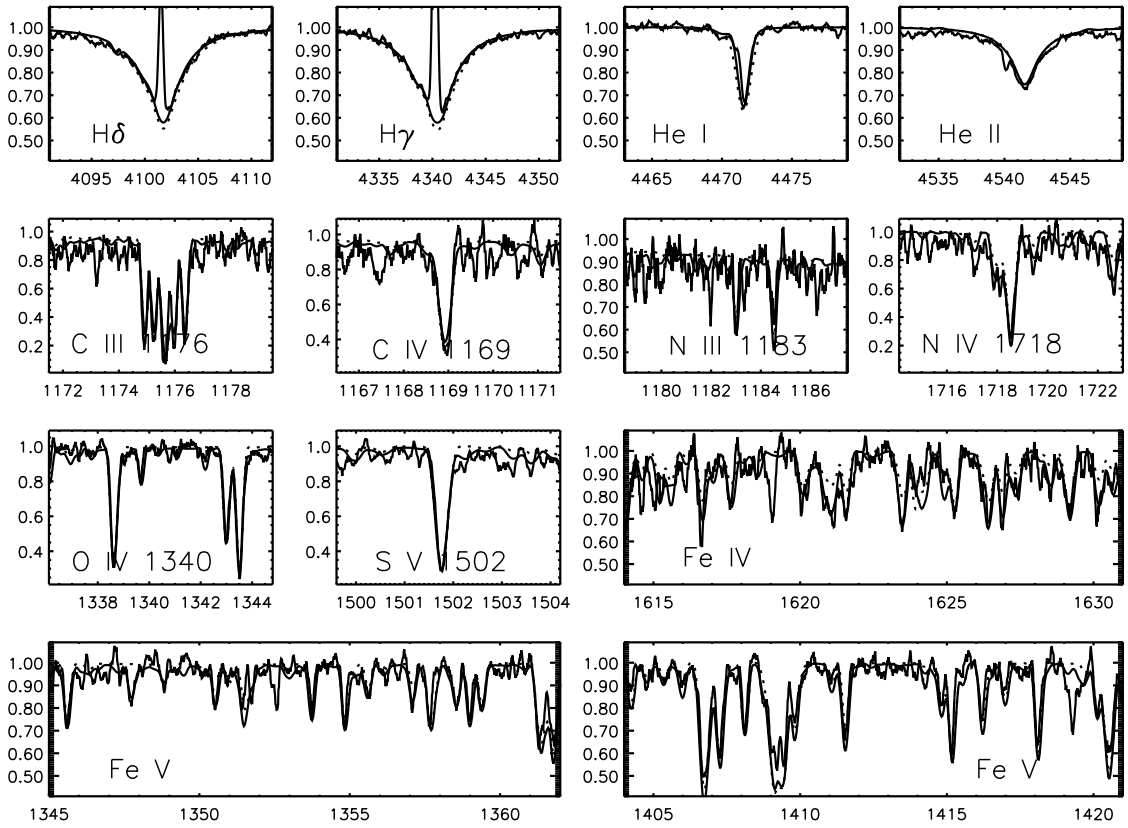

Fig. 7.— Best fits to MPG 113 photospheric lines used to derive the stellar parameters, $T_{\rm eff}$=40000 K, $\log g = 4.0$, and surface chemical composition, $Z/Z_{\odot} = 0.2$ (full line: TLUSTY, dotted line: CMFGEN).

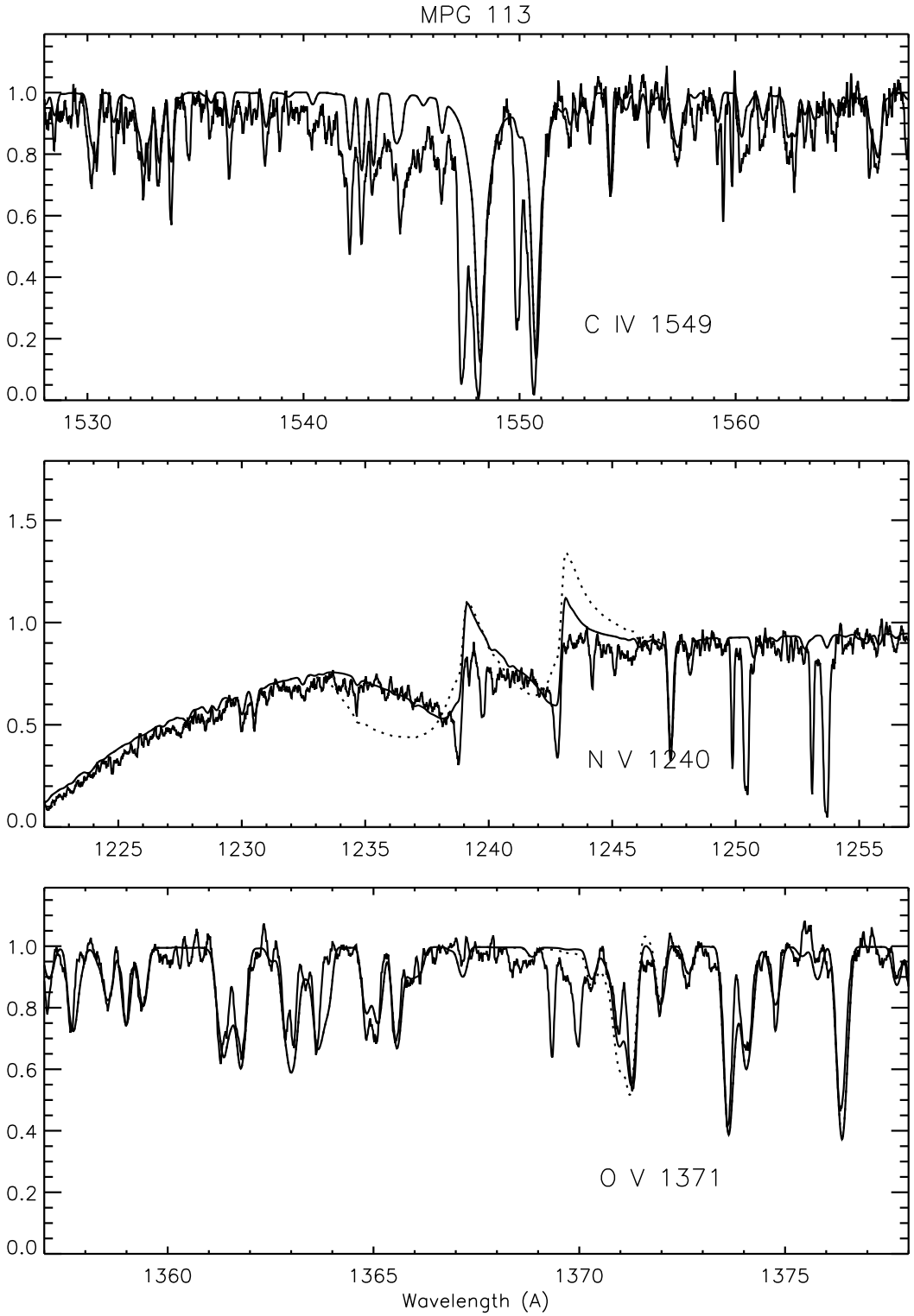

Fig. 8.— Influence of clumping on MPG 113 wind lines. A comparison of two models with different clump volume filling factors: no clumps, $f_\infty = 1.0$ (dotted); and best fit, $f_\infty = 0.1$ (full line). The mass loss rates are $\dot{M}= 3 \times 10^{-9}$, and $1 \times 10^{-9}\,\mathrm{M}_\odot\,\mathrm{yr}^{-1}$, respectively. The C IV lines predicted by the homogeneous and clumped wind models are almost identical (accounting for the different mass loss rates) and cannot be distinguished on this scale. The blue side of N V λ1240 is affected by interstellar Ly α absorption.

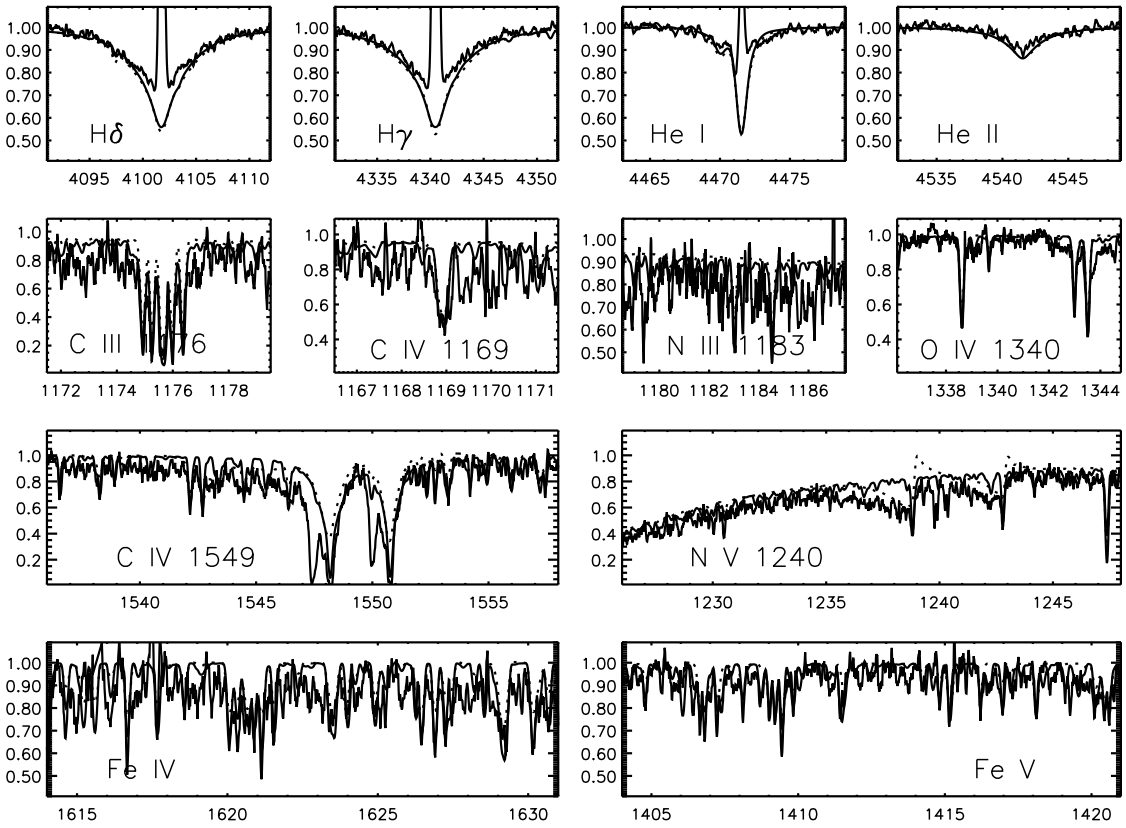

Fig. 9.— Best fits to MPG 487 photospheric lines used to derive the stellar parameters, $T_{\rm eff}$=35000 K, $\log g = 4.0$, and surface chemical composition, $Z/Z_{\odot} = 0.1$ (full line: TLUSTY, dotted line: CMFGEN).

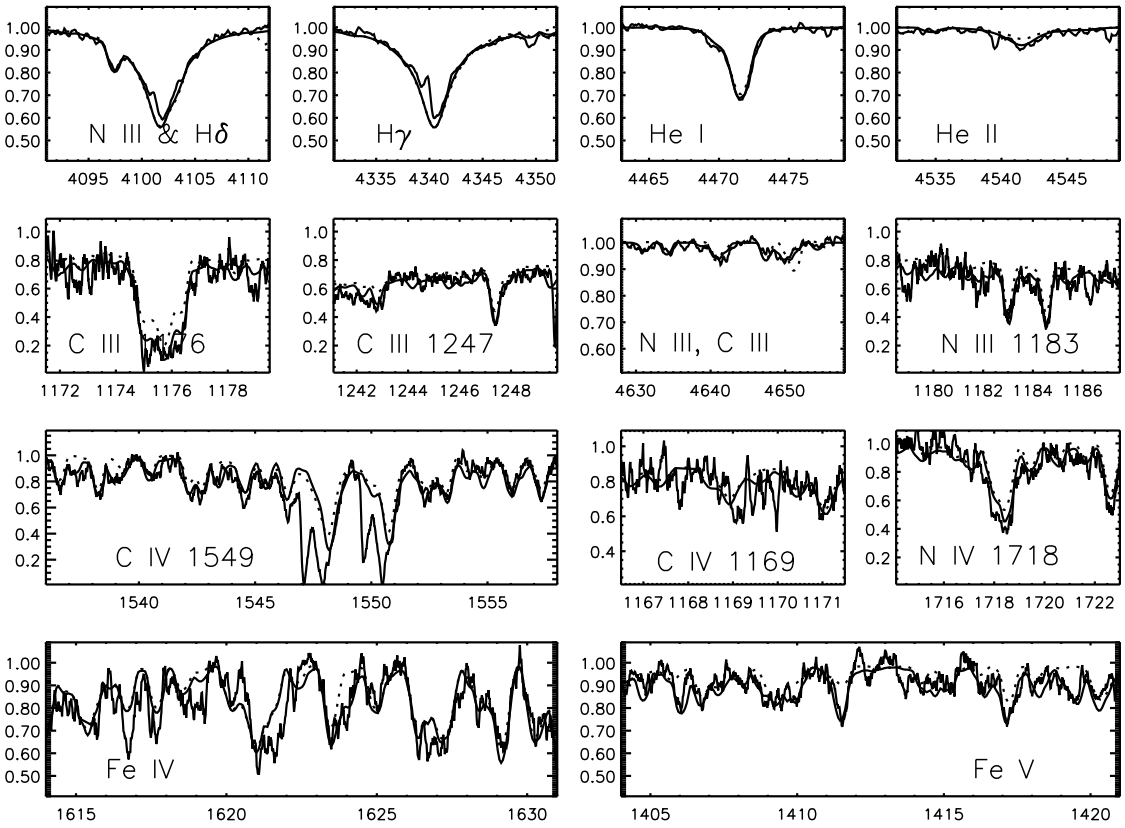

Fig. 10.— Best fits to MPG 12 photospheric lines used to derive the stellar parameters, $T_{\rm eff}$=31000 K, $\log g = 3.6$, and surface chemical composition, $Z/Z_\odot = 0.2$ (full line: TLUSTY, dotted line: CMFGEN).

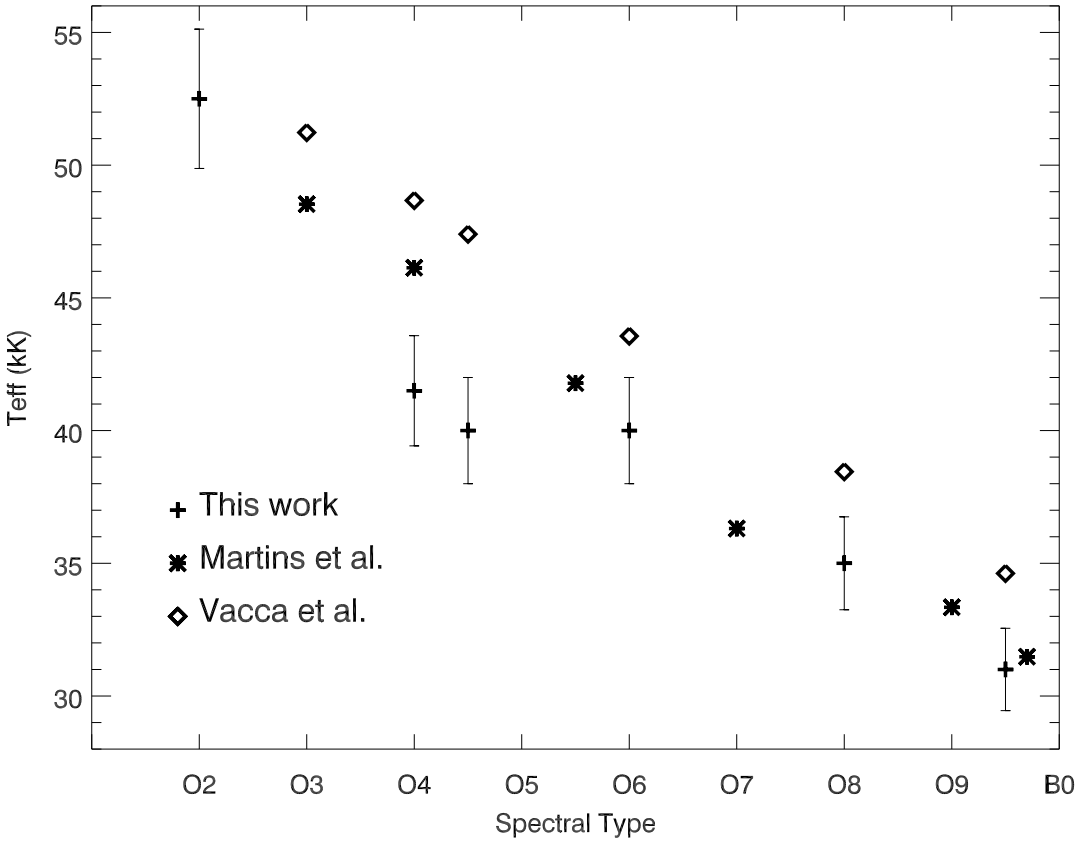

Fig. 11.— $T_{\rm eff}$ - Spectral Type relation for O dwarf stars from Vacca et al. (based on analyses of Galactic stars with unblanketed model atmospheres), from Martins et al. (based on blanketed CMFGEN model atmospheres with $Z = Z_{\odot}$), and from this study.

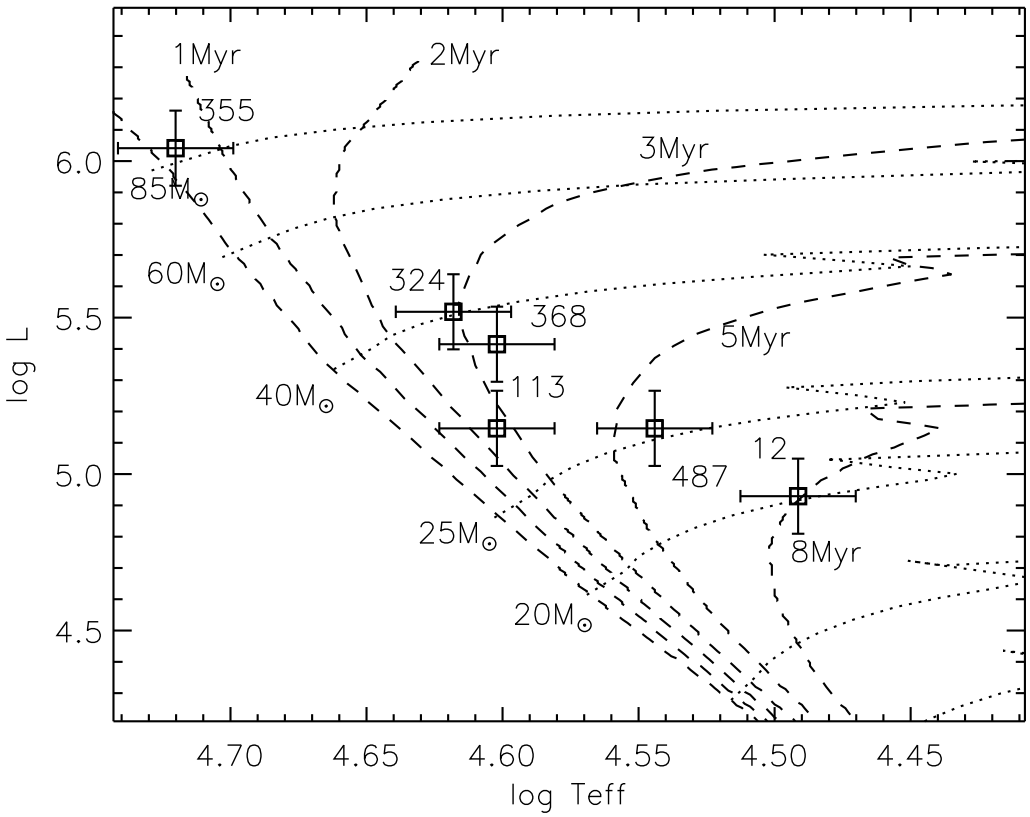

Fig. 12.— HR diagram with Geneva evolutionary tracks for a SMC metallicity, $Z/Z_{\odot} = 0.2$, and masses between 85 and 15 $M_{\odot}$ (dotted lines), and isochrones (ZAMS, 1, 2, 3, 5 and 8 10^6 yr; dashed lines). The large squares with error bars show our stellar sample in NGC 346.

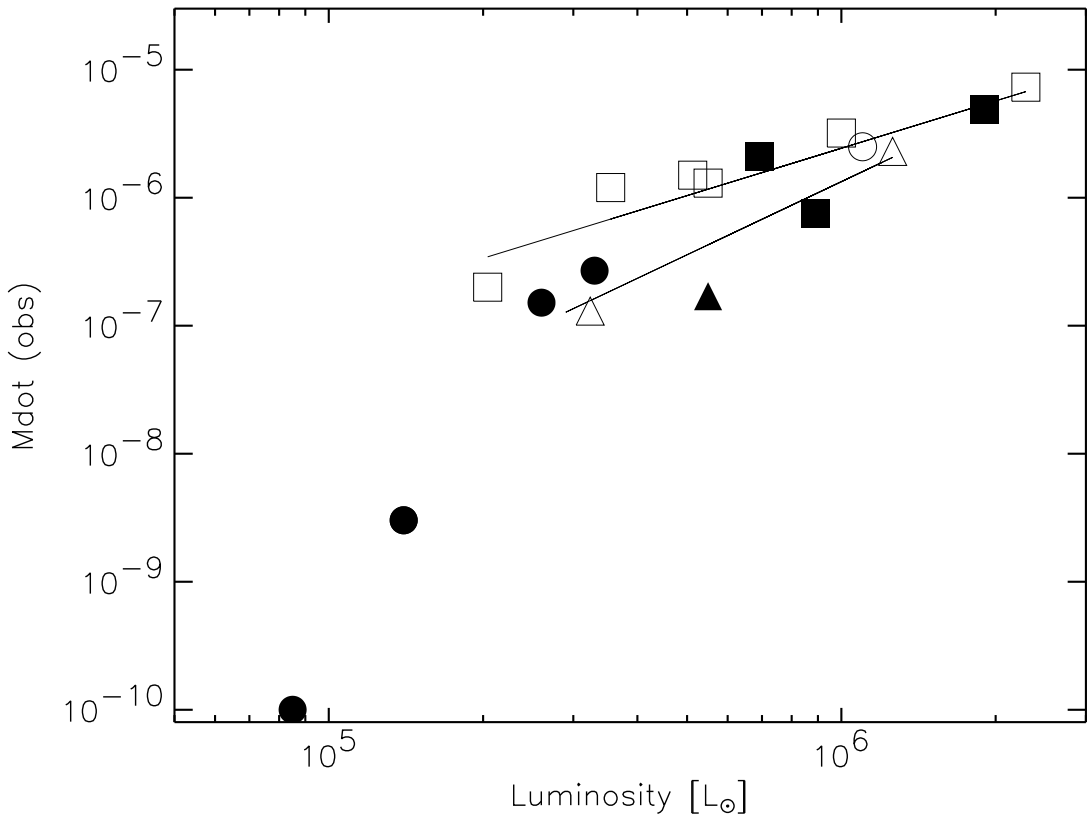

Fig. 13.— Measured mass loss rates for Galactic and SMC O stars as a function of the stellar luminosity: squares: Galactic stars, Puls et al. (1996); circles: SMC stars, this paper; triangles: SMC stars, Puls et al.; filled symbols: O dwarfs; empty symbols: O giants. Thin lines are least-squares fits for Galactic and SMC stars.

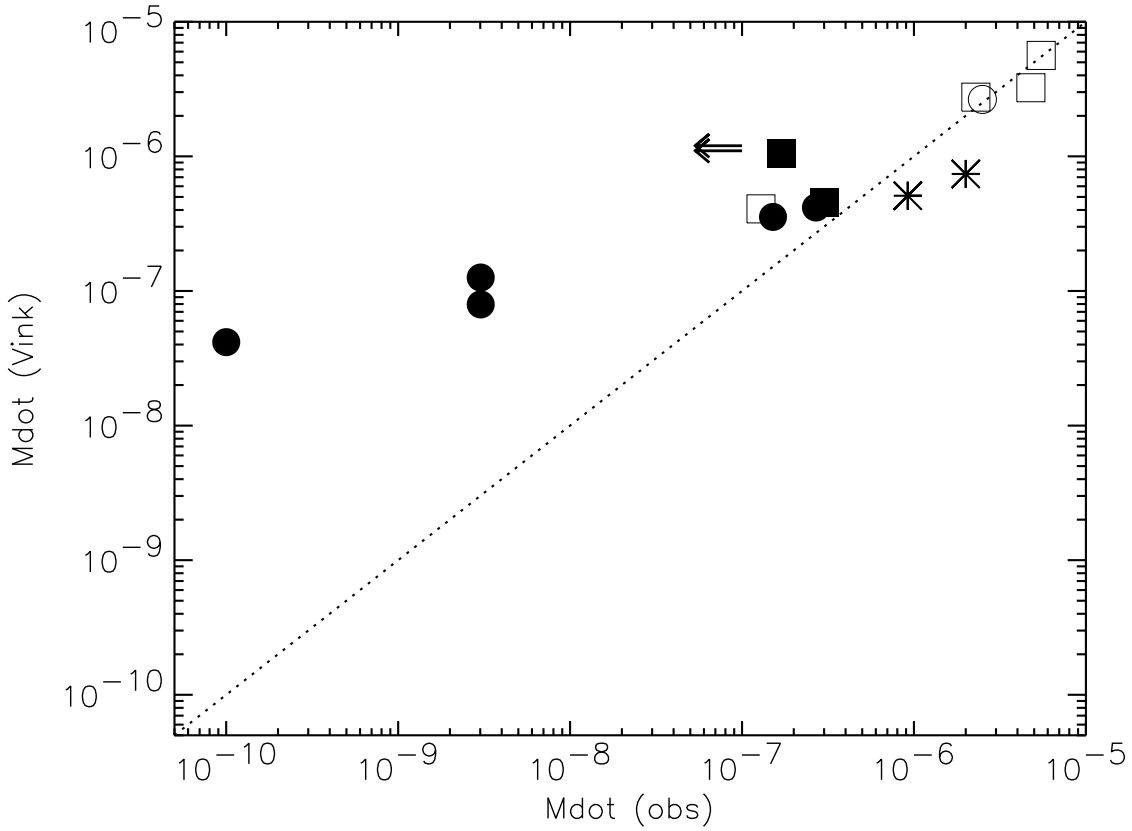

Fig. 14.— Comparison of measured and predicted mass loss rates for SMC O stars: circles: this paper; squares: Puls et al. (1996); stars: Hillier et al. (2003); filled symbols: O dwarfs; empty symbols: giant/supergiant O stars. The double arrow indicates an upper limit.

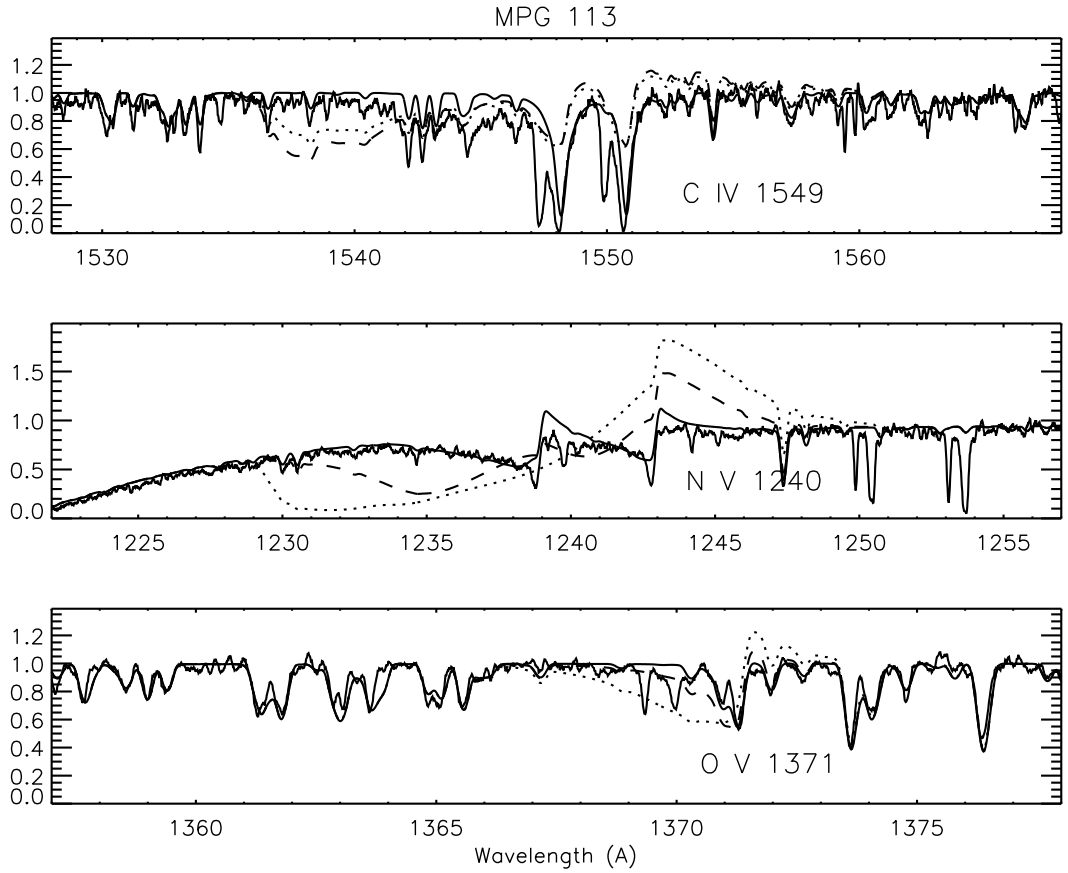

Fig. 15.— Predicted wind profiles for MPG 113, for an homogeneous ($f_\infty = 1.0$, dotted line) and a clumped wind ($f_\infty = 0.1$, dashed line), assuming Vink et al. theoretical mass loss rate ($\dot{M} = 10^{-7}\,\mathrm{M}_\odot\,\mathrm{yr}^{-1}$) and predicted terminal velocity, v_∞ =2225 $\mathrm{km\,s^{-1}}$. Because of the weak P Cygni profiles, v_∞ cannot be easily deduced from the observations. The best model fit (clumped wind, $f_\infty = 0.1$, $\dot{M} = 10^{-9}\,\mathrm{M}_\odot\,\mathrm{yr}^{-1}$) is also shown for comparison (full line).

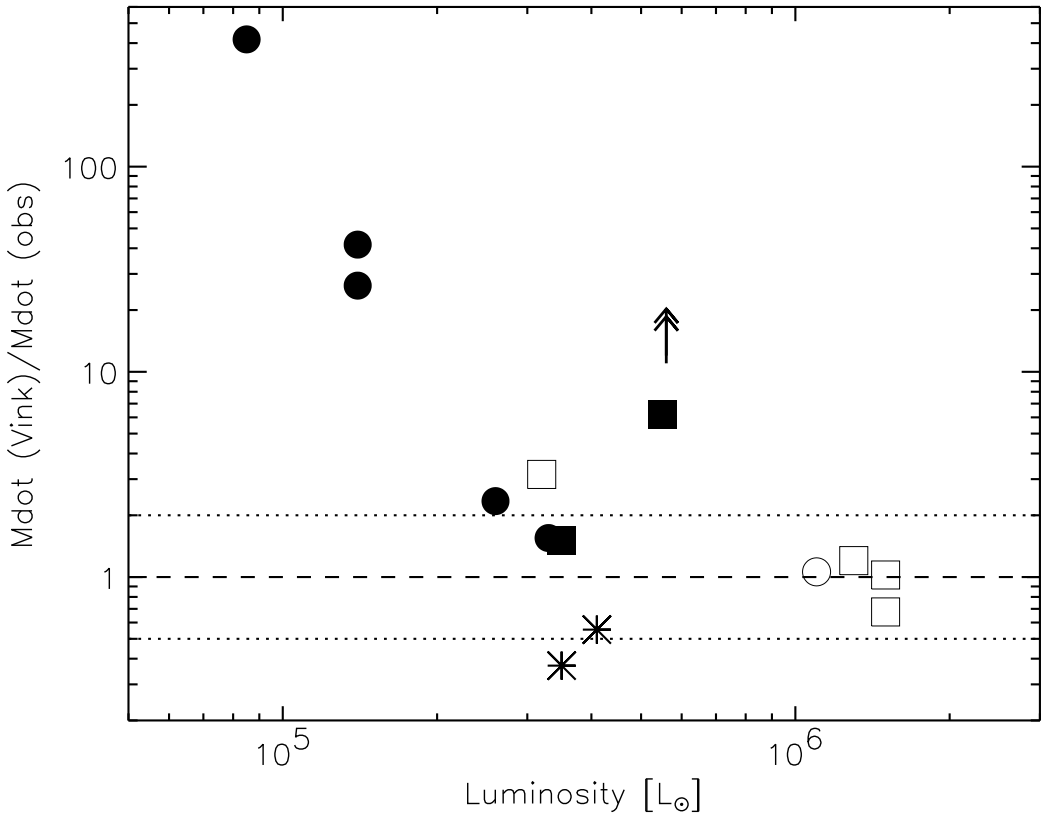

Fig. 16.— Ratio of predicted to observed mass loss rates for SMC stars as a function of the stellar luminosity. Symbols as in Fig. 14. The dotted lines indicate an agreement within a factor 2.

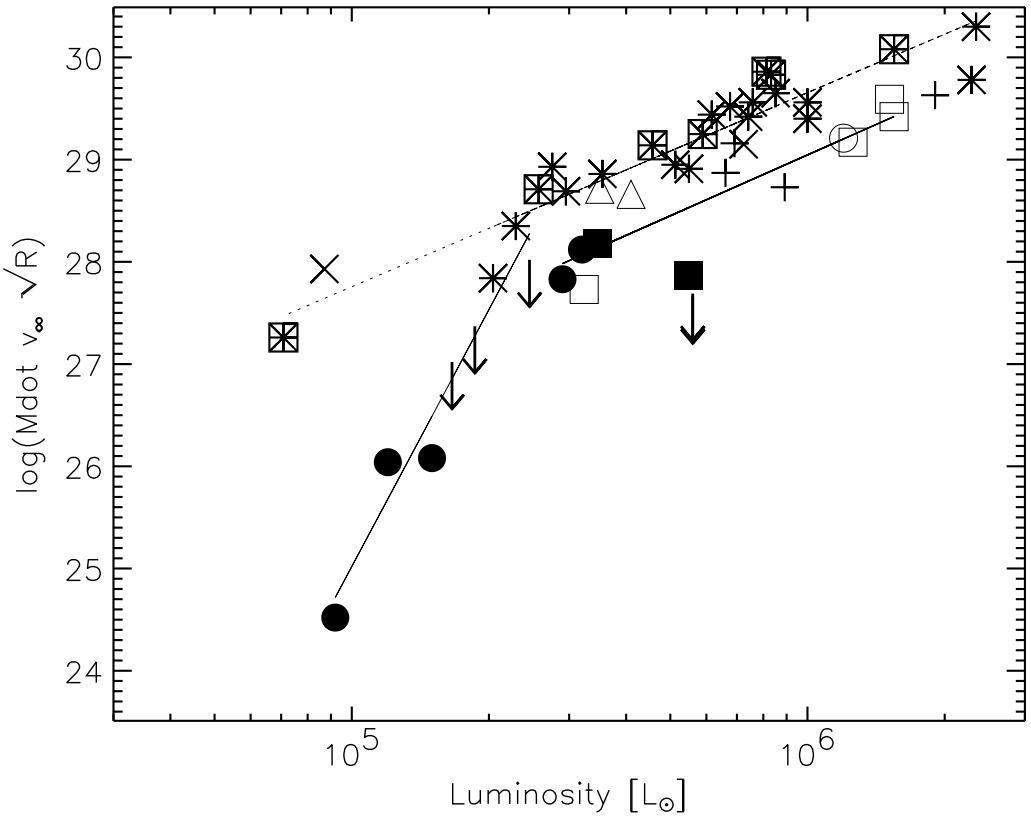

Fig. 17.— Modified Wind momentum-Luminosity relation for SMC and Galactic stars. SMC stars: this work (circles), Puls et al. (squares), Hillier et al. (triangles); filled symbols: O dwarfs, open symbols: O giants/supergiants. Galactic supergiants: Puls et al. (stars), Herrero et al. (stars within boxes), Kudritzki et al. (crosses); Galactic O dwarfs: Puls et al. (plusses). Arrows represent upper limits. Least-squares fits are shown for Galactic supergiants (top dotted line), SMC stars (lower full line), and low luminosity stars (steep line).

Table 1. Observational characteristics of the sample stars. Radial velocities have been measured from the optical and UV spectra. Color excesses have been derived from intrinsic colors of OSTAR2002 model atmospheres.

Star	Spectral Type	V	$B-V$	$E(B-V)$	V_r [km s^{-1}]	Telescope
NGC 346 MPG 355	O2 III (f*)	13.50	-0.23	0.06	165	AAT
NGC 346 MPG 324	O4 V((f))	14.02	-0.24	0.05	200	AAT
NGC 346 MPG 368	O4-5 V((f))	14.18	-0.23	0.05	150	AAT
NGC 346 MPG 113	OC6 Vz	14.93	-0.22	0.07	180	ESO
NGC 346 MPG 487	O8 V	14.53	-0.22	0.07	160	AAT
NGC 346 MPG 12	O9.5-B0 V (N str)	14.87	-0.15	0.12	220	ESO

Table 2. Model atoms included in TLUSTY and CMFGEN models.

Element	Ions	TLUSTY	CMFGEN
		Superlevels	
H	I, II	9, 1	20, 1
He	I, II, III	24, 20, 1	27, 22, 1
C	II, III, IV, V	22, 23, 25, 1	14, 30, 33, 1
N	II, III, IV, V, VI	26, 32, 23, 16, 1	0, 34, 44, 41, 1
O	II, III, IV, V, VI, VII	29, 29, 39, 40, 20, 1	24, 24, 29, 41, 13, 1
Ne	II, III, IV, V	15, 14, 12, 1	14, 23, 17, 1
Si	III, IV, V	30, 23, 1	20, 22, 1
P	IV, V, VI	14, 17, 1	36, 16, 1
S	III, IV, V, VI, VII	20, 15, 12, 16, 1	13, 51, 31, 28, 1
Fe	III, IV, V, VI, VII, VIII	50, 43, 42, 32, 1, 0	0, 100, 61, 57, 14, 1
Ni	III, IV, V, VI, VII	36, 38, 48, 42, 1	
		Individual Levels	
H	I, II	80, 1	30, 1
He	I, II, III	72, 20, 1	27, 30, 1
C	II, III, IV, V	44, 55, 55, 1	14, 54, 38, 1
N	II, III, IV, V, VI	71, 68, 58, 55, 1	0, 34, 70, 49, 1
O	II, III, IV, V, VI, VII	62, 116, 94, 89, 55, 1	25, 45, 48, 78, 13, 1
Ne	II, III, IV, V	29, 20, 18, 1	48, 71, 52, 1
Si	III, IV, V	105, 53, 1	34, 33, 1
P	IV, V, VI	14, 43, 1	178, 62, 1
S	III, IV, V, VI, VII	27, 15, 12, 34, 1	28, 142, 98, 58, 1
Fe	III, IV, V, VI, VII, VIII	12 660, 13 705, 11 986, 4 740, 1, 0	0, 1000, 300, 439, 153, 1
Ni	III, IV, V, VI, VII	11 335, 13 172, 13 184, 13 705, 1	

Table 3. Stellar parameters and chemical abundances derived for six O stars in NGC 346.

Star	MPG 355	MPG 324	MPG 368	MPG 113	MPG 487	MPG 12
Spectral Type	O2 III(f*)	O4 V((f))	O4-5 V((f))	OC6 Vz	O8 V	O9.5-B0 V (N str)
$T_{\rm eff}$ [K]	52500	41500	40000	40000	35000	31000
$\log g$ (cgs)	4.0	4.0	3.75	4.0	4.0	3.6
L $[L_\odot]$	1.1×10^6	3.3×10^5	2.6×10^5	1.4×10^5	1.4×10^5	8.5×10^4
$\xi_{\rm t}$ [km s^{-1}]	25	15	15	10	2	5
$V \sin i$ [km s^{-1}]	110	70	60	35	20	60
Homogeneous winds						
$\dot{M}$ [M$_\odot$ yr^{-1}]	2.5×10^{-6}	2.7×10^{-7}	1.5×10^{-7}	3×10^{-9}	3×10^{-9}	1×10^{-10}
v_∞ [km s^{-1}]	2800	2300	2100	$\geq$1250	$\geq$1100	$\geq$1000
β	0.8	1.0	1.0	1.0	1.0	1.0
Clumped winds						
f_∞	0.01	0.1	0.05	0.1		
$\dot{M}$ [M$_\odot$ yr^{-1}]	1.8×10^{-7}	1.0×10^{-7}	5.7×10^{-8}	1×10^{-9}		
Abundances[a]						
y (He/H)	0.1	0.1	0.1	0.1	0.1	0.1
C/C$_\odot$	0.2	0.06	0.06	0.1	0.1	0.06
N/N$_\odot$	1.0	0.2	0.6	0.2	0.03	1.0
O/O$_\odot$	0.2	0.2	0.2	0.2	0.2	0.2
Si/Si$_\odot$	0.2	0.2	0.2	0.2	0.1	0.2
S/S$_\odot$	0.2	0.2	0.2	0.2	0.1	0.2
Fe/Fe$_\odot$	0.2	0.2	0.2	0.2	0.1	0.2
Evolutionary status[b]						
Age [10^6 yr]	<1 ?	$\approx$3	$\approx$3	$\approx$3	$\approx$5 ?	$\approx$8
$M_{\rm evol}$ $[M_\odot]$	90 ?	40	38	33	25 ?	21
$M_{\rm spec}$ $[M_\odot]$	64	44	26	24	32 ?	16
N/C[c]	10	6	20	4	0.6	30

[a]Solar abundances from Grevesse & Sauval (1998).

[b]Question marks indicate doubtful values, see further discussion in §6.3.

[c]Abundance ratio relative to the SMC nebular ratio, N/C$\approx$0.16 (Venn 1999).

Table 4. Stellar parameters and predicted mass loss rates from Vink et al. (2001). Terminal velocities in parentheses are calculated as twice the escape velocities.

Star	$T_{\rm eff}$ [K]	$\log L$ [$L_\odot$]	M [$M_\odot$]	$v_{\rm esc}$ [$\rm km\,s^{-1}$]	v_∞ [$\rm km\,s^{-1}$]	$v_\infty/v_{\rm esc}$	$\log \dot{M}$(obs) [$\rm M_\odot\,yr^{-1}$]	$\log \dot{M}$(Vink) [$\rm M_\odot\,yr^{-1}$]
MPG 355	52500	6.04	65	1033	2800	2.71	−5.6	−5.6
MPG 324	41500	5.51	40	1053	2300	2.18	−6.6	−6.4
MPG 368	40000	5.41	40	1041	2100	2.02	−6.8	−6.4
MPG 113	40000	5.13	30	1112	(2225)	2.00	−8.5	−6.9
MPG 487	35000	5.13	25	939	(1880)	2.00	−8.5	−7.1
MPG 12	31000	4.93	20	795	(1590)	2.00	−10.0	−7.4